Contribution of Fresh Submarine Groundwater Discharge to the Gulf of Alaska

A. A. Russo[1,2], D. F. Boutt[2], L. A. Munk[1], J. Jenckes[1]

[1]Department of Geological Sciences, University of Alaska Anchorage, Anchorage, AK, USA

[2]Department of Geosciences, University of Massachusetts Amherst, Amherst, MA, USA

Corresponding author: Aeon Russo (arusso3@alaska.edu)

Key Points:

- We compare two water balance approaches to estimate fresh submarine groundwater discharge to the Gulf of Alaska
- Mean annual flux of fresh, terrestrial groundwater ranges from 26.5 to 86.8 km^3, or 3.5-11.4% of the total annual freshwater discharge
- We identify fresh submarine groundwater discharge hotspots from an extensive remote high-latitude coastline

Abstract

High latitude mountain environments are experiencing disproportionately adverse effects from climate change. The Gulf of Alaska (GoA) region is an embodiment of this change, particularly concerning a shifting hydrologic balance. Even so, the magnitude and contribution of fresh submarine groundwater discharge (fresh SGD) remains virtually unexplored within the region, though it has gained increasing attention globally due to its chemical significance and influence on coastal ecosystems. Here we provide the first regional estimates of fresh SGD to the GoA using two established water balance approaches. This is an effective way to distinguish the contribution of terrestrially derived fresh SGD, rather than the more commonly quantified total SGD which includes discharge that is driven by marine forces such as sea-level oscillations and density gradients. We compare the approaches and assess their capabilities in computing the magnitude of fresh SGD over a large regional scale. Mean annual fresh SGD flux ranges between 26.5 to 86.8 $km^3\ yr^{-1}$ to the GoA, equivalent to 3.5-11.4% of the total freshwater discharge. Contributions are highest in the Southeastern panhandle and lowest in the Cook Inlet basin, with the highest area normalized contribution occurring in the Prince William Sound. Fresh SGD exhibits high spatial and temporal variability throughout the region. Although freshwater discharge to the GoA is investigated considerably, the importance of fresh SGD has, thus far, been overlooked.

Plain Language Summary

Mountainous regions are highly susceptible to the impacts of climate change. This is especially evident in the Gulf of Alaska (GoA), where freshwater systems flowing from mountainous coastlines are experiencing a rapid shift in the timing, quantity, and chemical composition of their waters as they outflow to the ocean. Fresh submarine groundwater discharge (fresh SGD) is one such pathway that water travels where water below the ground surface empties into the ocean underneath the ocean's surface. This type of water flow is known to have elevated nutrients and solutes, thus making it important for near shore marine life. We estimate fresh SGD to the GoA using two mathematical models and compare the results from each. We find that fresh SGD is between 3.5-11.4% of the total amount of freshwater that flows to the ocean from the GoA, which is a significant portion.

1 Introduction

Coastal mountain ranges at high-latitudes harbor critical environments and productive ecosystems that provide unique resources to both local and global communities (Bunn et al., 2007; O'Neel et al., 2015). Rugged terrains rising abruptly from the ocean possess the capability to harness and recruit large volumes of water to the terrestrial domain. Representative features, such as a low-temperature climate regime and higher elevations, also enable the development of the cryosphere where large reserves of freshwater may be stored, allowing these distinct settings to hold a substantial influence over global-scale processes (Chiang and Bitz, 2005). Unfortunately, these highly active coastal landscapes are experiencing disproportionately enhanced physical and ecological changes in a currently warming climate (Portner et al., 2019; Arp et al., 2020). Such changes are particularly pronounced in the Gulf of Alaska (GoA), where dramatic shifts in precipitation patterns, temperature, and glacier volume loss are well underway (Arendt et al., 2002; O'Neel et al., 2015; Beamer et al., 2017; Arp et al., 2020).

The freshwater flux driven by rainfall and the melting of snow and ice from the GoA is receiving increasing attention from both the scientific community and the public. This should come as no surprise for a regional basin that only encompasses 1.7% of the total land area of North America, and yet yields over 12% (Royer, 1982; Wang et al., 2004; Neal et al., 2010; Hill et al., 2015; Beamer et al., 2016) of the total continental discharge (Syed et al., 2009). The freshwater flux will only continue to increase in magnitude in the coming decades due to rapid glacier retreat that rivals among the largest volumetric losses observed globally (Arendt et al., 2002; Gardner et al., 2013; Beamer et al., 2017). Additionally, forecast modeling predicts that the current rise in temperatures will result in increasing precipitation, most notably in the form of fall and winter rains (Beamer et al., 2017). This immense hydrologic discharge transports with it an abundance of terrigenous materials, including sediments, solutes and nutrients, that mediate marine ecosystems (Hood et al., 2009; Edwards et al., 2021; Jenckes et al., 2021) and retain a dominant influence on local and regional oceanographic processes (Weingartner et al., 2005). Consequently, considerable efforts have been made on estimating both the freshwater (Neal et al., 2010; Beamer et al., 2016) and chemical (Brown et al., 2010; Schroth et al., 2011; Brennan et al., 2014; Hood et al., 2015; Jenckes et al., 2021) flux from rivers to the GoA. However, there is

one major component of the freshwater and nutrient flux to the GoA that remains virtually unexplored. The missing piece is coastal groundwater.

Coastal aquifers are especially vulnerable to the impacts of a warming planet (Ferguson and Gleeson, 2012). Groundwater may act as a temporary buffer against climate-mediated alterations to the hydrologic budget within mountain belts (Somers et al., 2019; Mackay et al., 2020). When compared with proximal surface waters, groundwater within coastal aquifers is chemically enriched (Slomp and Van Cappellen, 2004; Beck et al., 2013; Rahman et al., 2019; Mayfield et al., 2021). Subterranean estuaries, a coastal aquifer in which meteoric groundwater mixes with infiltrating seawater, are known to be biogeochemical reaction hotspots (Moore, 1999). These nutrient-laden waters eventually enter the ocean through the porous media of the seafloor via diffuse, non-point pathways. This flux is termed submarine groundwater discharge (SGD) and includes the flow of any water, regardless of the origin or chemical composition, that discharges to the ocean from below the oceanic surface (Burnett et al., 2006). This definition includes both seawater that is recirculated by oceanographic processes, such as wave set-up and tidal pumping, and meteoric groundwater driven by the terrestrial gradient. The latter is also known as fresh SGD (fresh SGD). Local, regional, and global estimates of fresh SGD are highly variable, though they typically range from 1-10% of river discharge to the ocean (Taniguchi et al., 2019). Zhou et al. (2019) estimate that high latitude, active margins have fresh SGD rates approximately double that of the global average. Additionally, islands have been observed to have higher groundwater discharge rates per unit area than continents (Hajati et al., 2019). If these findings prove to be accurate, higher fresh SGD rates are expected from the mountainous, high latitude coast of the GoA which is occupied by an abundance of island archipelagos. Few studies have estimated this flux in high latitude mountain regions, much less within the subpolar domain. Further, fresh SGD estimates have mainly been provided for relatively short time periods or calculated as a long-term mean. This limits our understanding of how this flux is trending both locally and globally.

Developing a complete understanding of the freshwater and geochemical budgets in the GoA, as well as their sensitivities to climate-mediated changes, must include SGD as a vital component. SGD plays an influential role across marine biota in a range of coastal ecosystems (Lecher and

Mackey, 2018), with positive impacts observed on primary productivity (Lecher et al., 2017), denitrification (Erler et al., 2014), enhanced growth rates in mussels and oysters (Chen et al., 2018; Andrisoa et al., 2019; Spalt et al., 2020), and enhanced productivity and abundance observed in fisheries (Fujita et al., 2019; Pisternick et al., 2020; Starke et al., 2020). SGD may also contribute to unfavorable impacts, such as eutrophication (Beusen et al., 2013), harmful algal blooms (Hu et al., 2006), deoxygenation (Peterson et al., 2016), and pollutant loading (Knee and Paytan, 2012). Nitrogen fluxes associated with SGD exceed river inputs in ~60% of the cases in a recent review from Santos et al. (2021). Higher alkalinity associated with groundwater may also enlist fresh SGD as an important buffer against ocean acidification (Cyronak et al., 2013). The coastal margins of the GoA offer an extensive passageway for these nutrients and solutes to enter the ocean by means of SGD. Groundwater is likely a critical element in the robust coastal ecosystems and wild fisheries within the GoA, thus quantifying the nutrient and freshwater flux driven by SGD is of great importance to coastal water management (Robinson et al., 2018). However, while surface waters can be more accessible to sample and evaluate, it remains a challenge to quantitatively constrain the rate and timing of SGD as this flux varies significantly in both time and space in this remote region.

Methods to detect and evaluate SGD have enrolled a suite of multidisciplinary approaches (Taniguchi et al., 2019). These include thermal imaging to identify SGD hotspots (Wilson and Rocha, 2012; Tamborski et al., 2015), electromagnetic sensing to discern the saltwater-freshwater interface (Swarzenski et al., 2007b), instrumentation that measures discharge directly (e.g. seepage meter; Taniguchi, 2002; Ronayne et al., 2012), tracer techniques (Swarzenski et al., 2007a; Santos et al., 2009; Michael et al., 2011; Rodellas et al., 2015), and hydrologic models, such as water balance calculations (Sawyer et al., 2016; Sugimoto et al., 2016) and dual-density numerical flow models (Xin et al., 2010; Kuan et al., 2012; Heiss and Michael, 2014; Michael et al., 2016). Currently, the only estimates of SGD in the GoA region are from two small gravel-dominated beaches where it was identified to be a significant source of carbon, nitrogen, silicon, iron, and nickel (Dimova et al., 2015; Lecher et al., 2016). These studies reported SGD rates ranging from 130 ± 180 cm day^{-1} to 120 ± 50 m^3 m^{-1} day^{-1} estimated using radon and radium activity, respectively (Dimova et al., 2015; Lecher et al., 2016). The authors were unable to isolate fresh SGD from total SGD with the tracer methods they employed. The current study

focuses on regional fresh SGD to the GoA, which has not previously been explored. As mentioned earlier, two common approaches to estimate fresh SGD are water budgets that apply lumped parameters to model domains and groundwater flow models with high resolution input. Zhou et al. (2018) compared these two generalized approaches over the large domain of the U.S. Atlantic and Gulf Coasts. The water balance model, although computationally inexpensive, is unable to resolve flow paths or continuous distributions. The numerical flow model allows for the incorporation of heterogeneous geologic features but comes at the price of long model run times. Additionally, numerical groundwater simulations cannot be applied to areas that lack geologic and hydrogeologic observations (Zhou et al., 2018). Further, the majority of fresh SGD models are steady state and do not account for seasonal variability. Previous studies have identified high temporal variability associated with the seasonality and lag time of fresh SGD (Michael et al., 2005; Charette, 2007; Smith et al., 2008; Klammler et al., 2020).

This study is the first to calculate the flux of regional fresh SGD to the GoA by applying two distinct lumped parameter water balance approaches. Both approaches calculate this flux for individual, unmonitored coastal catchments across the entire GoA domain. These types of approaches allow us to discern the contribution of fresh SGD from that of the more commonly quantified total SGD. This is important to distinguish when the quantity of freshwater delivered to the coast is essential information, such as for oceanographic and ecological models. The first model partitions each coastal catchment into a three-layer system that accounts for topsoil-subsoil-aquifer interactions with lumped daily hydrologic inputs and hydrogeologic parameterization derived from modeled or remotely measured regional and global datasets. Fluxes are provided at a daily timestep. Computational time is greatly reduced by leveraging an existing high-resolution, long-term hydrologic model that accounts for regionally specific hydrologic processes that have not been considered in previous water balance approaches. The second model approximates net recharge using rates derived from global land surface models acquired from NASA's Global Land Data Assimilation System (GLDAS) and distributes them over individual coastal catchment recharge zones. Using two unique computational approaches allows for inter-model comparisons and estimations of uncertainty in the absence of appropriate validation datasets. We compare the simplifying assumptions in each computational method and the subsequent fresh SDG estimates. Both models provide the first regional estimates for fresh

SGD to the GoA and identify the locations of hot spots. We also present daily, seasonal, and annual variations in fresh SGD to the GoA over the 35-year model period.

2 Study Area

The GoA is an important region to study SGD due to its steep topographic gradient, extremely wet climate, presence of glaciers, minimal anthropogenic extraction or influence, and favorable geologic media in the form of highly fractured bedrock and coarse, proglacial sediments. These conditions typically lend themselves to high groundwater, and thus nutrient and solute, fluxes (Zhou et al., 2019; Adyasari et al., 2019). The GoA watershed occupies an area of 419,127 km^2 stretching from Cape Igvak on the Alaska Peninsula and Kodiak Island to the border with British Columbia, Canada at the Portland Inlet. This landscape is home to the northern Pacific Coastal Temperate Rainforest, the northern-most rainforest on Earth (O'Neel et al., 2015). Additionally, four major snow and ice covered mountain ranges span the coastline and encompass extensive estuaries, fjords, and glaciofluvial deltas. This influences the GoA region to be largely remote and inaccessible, with a total population of 433,179 predominately located in dense population centers and economic regions (live.laborstats.alaska.gov/pop/index.cfm, last accessed 21 December 2022) but also including many Alaska Native villages that have a high dependance on coastal regions and resources for subsistence.

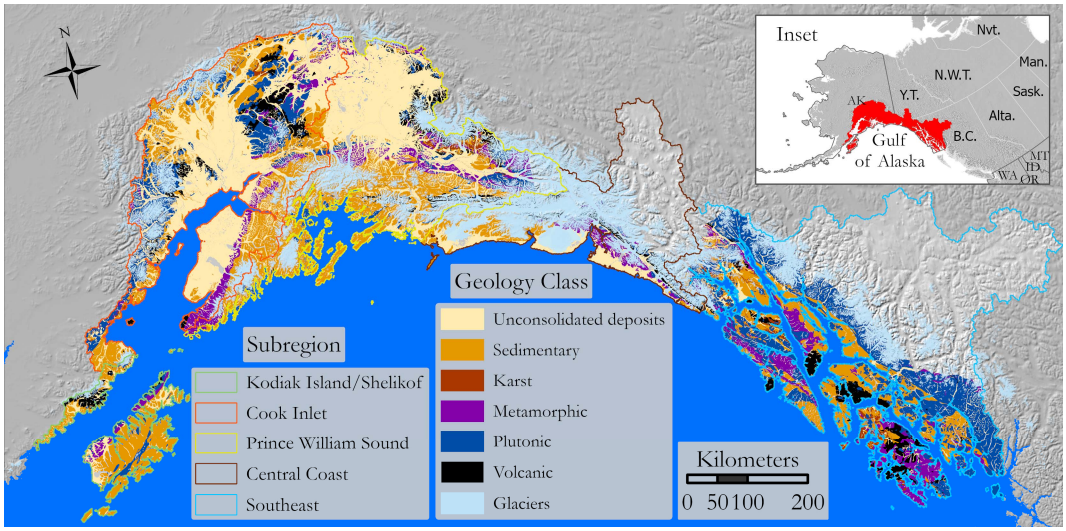

191 **Figure 1**. Regional distribution of major lithologic classes across the Gulf of Alaska drainage
192 basin. Rock units provided by the USGS Geologic Map of Alaska (Wilson and Labay, 2016) are
193 grouped using custom Python scripts. Lithologic units are not provided for areas within Canada.
194 The Gulf of Alaska drainage basin is further separated into 5 geographic subregions.
195
196 We divide the GoA drainage basin into five geographic subregions due to the distinct ecological
197 zones and hydrogeologic properties and inputs therein (Figure 1). From west to east, these
198 subregions are Kodiak Island and the Alaskan Peninsula along the Shelikof Straight, the Cook
199 Inlet Basin, Prince William Sound, the Central Coast, and the Southeast panhandle. Each region
200 holds a combination of unique streamflow patterns that reflects varying contributions from rain,
201 snow, and glacial ice (Sergeant et al., 2020). Further, we focus this study on the coastal
202 catchments, the wedges of land in between watersheds draining to streams and rivers, within
203 each subregion. The coastal catchments along the GoA coastline are generally characterized by
204 steep topography, lush vegetation, and abundant wildlife. These are economically important
205 regions due to the richness of their fisheries and attractiveness for tourism and adventure travel
206 (Munro and Gill, 2006; Stopha, 2017). The coastal catchments are mostly zoned in a wet and
207 mild maritime climate (Bieniek et al., 2014). The majority of their precipitation arrives in the
208 autumn as rain and continues through the winter as snow, with notable variation across the major
209 subregions (McAfee et al., 2013). The Cook Inlet Basin and Kodiak Island/Shelikof subregions
210 receive far less precipitation than the subregions to the west, with Central Coast receiving the
211 greatest precipitation with yearly means of around 3 meters (Table 1). These coastal catchments
212 are extensive, spanning a total of 28,069 kms of coastline and containing 9.2% of the total
213 contributing land area of the GoA (Table 1). The steep terrain produces mean slopes in excess of
214 30% in the Southeast subregion, and averages 5.7% across all coastal catchments. Elevations
215 range from sea level to a maxima of 3048 meters in the Prince William Sound, with a mean
216 elevation of 176 meters. The land cover of coastal catchments along the GoA is mostly forested
217 (47.1%), with an additional mixture of grassland/shrub (26.4%), bare soil/rock (24.8%), and
218 snow/ice (1.6%), derived from the North America Land Cover Characteristics Data Base, version
219 2.0 (https://www.usgs.gov/media/images/north-america-land-cover-characteristics-data-base-
220 version-20, last accessed 13 December 2022). Land described as urban and built-up covers less

than 0.06% of the coastal catchments. An overview of coastal catchment characteristics divided by subregion are provided in Table 1.

Table 1. Coastal catchment characteristics and summary statistics listed by subregion

Coastal catchment variable	Southeast	Central Coast	Prince William Sound	Cook Inlet	Kodiak Island/ Shelikof	GoA Total
Count	6594	727	2494	1105	1976	12896
Mean annual precipitation (mm)	2550.4	2989.2	2576.8	872.4	1539.4	2181.0
Area (km^2)	19861	2429	6897	3714	5749	38650
Percent regional area	12.2%	4.2%	7.8%	3.6%	30.4%	9.2%
Coastline length (km)	14448	1550	5751	2153	4167	28069
Mean drainage length (m)	1763.6	2022.9	1575.2	2162.1	1762.9	1857.3
Mean slope (%)	5.9	3.6	6.2	4.6	5.3	5.1
Mean elevation (m)	179.9	118.0	202.5	146.6	165.1	162.4
Max elevation (m)	2072.0	2072.0	3048.0	1339.0	1164.0	3048.0
Land Use Land Cover (%):						
Forested	73.6%	41.4%	15.2%	33.9%	13.9%	47.1%
Grassland/Shrub	5.8%	9.4%	28.8%	45.8%	83.3%	26.4%
Bare Soil/Rock	19.7%	44.2%	51.8%	19.7%	2.6%	24.8%
Snow/Ice	0.06%	5.05%	4.21%	0.06%	0.20%	1.62%
Developed	0.01%	0%	0%	0.48%	1.02%	0.06%

Temperate, active coastal margins are proposed to supply the largest provenance of terrigenous materials to the oceans globally, with the GoA being considered as the greatest contributor of sediment to the Pacific Ocean from either North or South America (Jaeger et al., 1998). Coarse hydrostratigraphic units like colluvium, alluvial fans, outwash plains and glaciofluvial deltas provide important reservoirs and efficient flowpaths for mountain groundwater (Mackay et al., 2020). These environments can deposit facies that are hundreds of meters thick and extend tens of kilometers laterally (Maizels, 1993). The input to fresh SGD from these unconsolidated units are coupled with the complex bedrock geology of the region, with shallow, weathered, and deep fracture networks, all of which have been further enhanced by rapid isostatic depression and

rebound from multiple glaciations (Bradley and Kusky, 1990; Larsen et al., 2005). These are the effective mediums through which fresh SGD travels to the GoA from the coastal catchment domain of this study. A generalized geologic map of the region modified from the USGS Geologic Map of Alaska (Wilson and Labay, 2016) is given in Figure 1 and classifies units into major lithologic classes. Coastal catchments of Kodiak Island/Shelikof and the Prince William Sound are dominated by siliceous sedimentary facies, Cook Inlet and the Central Coast are dominated by unconsolidated deposits, and the Southeast exhibits the highest variability in rock types along the coast. Karst facies are the least represented, and are only extant along the coastline of the Southeast and the western Cook Inlet.

3 Data and Methods

3.1 General Overview and Conceptualization

We calculate historical fresh SGD using two previously adopted water budget approaches (Sawyer et al., 2016; Zhou et al., 2018, 2019; Hajati et al., 2019) for 35 years between 1979 and 2014 for 12896 coastal catchments of the GoA watershed. Here we describe coastal catchments as the land areas that remain after watersheds draining to stream networks have been delineated (Figure 2). These medial land areas outside of surface water catchments act as the recharge zones from which fresh SGD flows diffusely to the coast, whereas streams and rivers discharge water from discrete, observable outlets. Following extensive manual comparisons between 1:24,000-scale hydrography maps and satellite imagery, we chose a contributing area threshold of 20 km^2 to isolate coastal catchments. Coastal land areas beneath this threshold are observed in aerial imagery to be the wedge-shaped stretches of coastline that are devoid of streams between watersheds that flow to streams. The larger watersheds containing streams likely contribute to fresh SGD (Yu et al., 2021), but research estimating their influence is limited and impractical for the scale of this study. By eliminating these larger watersheds that contain streams, we may apply the simplifying assumption that all water recharged to the coastal aquifer will become fresh SGD along the coast. Furthermore, this threshold almost entirely eliminates the influence from the 49 tidewater glaciers along the GoA coastline, although they are also likely to contribute additionally to the groundwater flux (Boulton and Caban, 1995; He et al., 2022). Our threshold is similar to previous studies that use HydroSHEDS (Lehner et al., 2008) to define coastal recharge zones (Zhou et al., 2018, 2019), and is smaller than the majority of recharge

areas applied to regional fresh SGD estimates, which can be as high as 81 km^2 (Hajati et al., 2019). The GoA coastline is occupied by 13,017 of these coastal catchments. Datasets that apply lumped aquifer parameters to each coastal catchment do not have complete coverage, resulting in the removal of 120 coastal catchments from model calculations. We use the USGS Hydro1K North America digital elevation model (https://earthexplorer.gov/) to generate the stream network, calculate the slope and the mean and max elevations of the catchments, and to delineate the coastline.

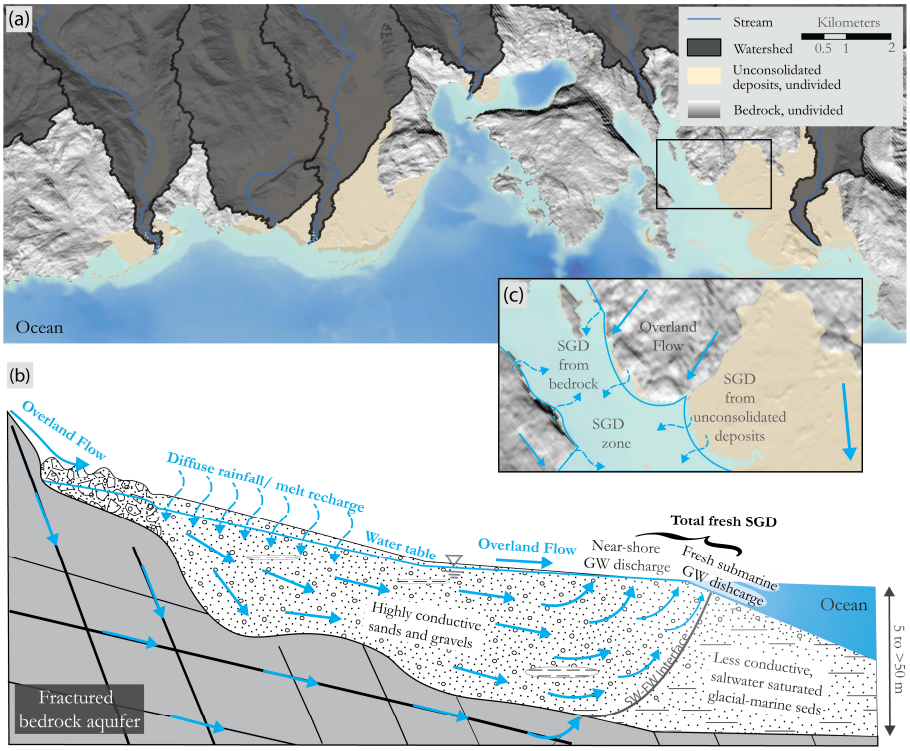

Figure 2. A graphical representation of coastal catchment geology, geometry, and freshwater dynamics in the Gulf of Alaska margin. (a) Representative example of the regional coastline. Watersheds draining to streams are shaded in gray to expose the coastal catchments that remain between. Unconsolidated deposits are shown in beige. A generated hillshade model represents the undivided bedrock geology. SGD zones in the shallow ocean are shaded in turquoise; (b) conceptual model of groundwater recharge, flow, and discharge along geologic cross section from mountains to sea. Fresh meteoric groundwater is discharging to the ocean from unconsolidated sediments in this example, but fractured bedrock aquifers are also depicted as

they are represented and distributed throughout the domain of the models; (c) schematic plane view (inset from (a)) of water flow and SGD from a coastal catchment.

Within each coastal recharge area, rain, snow- and ice-melt that does not become lost due to evapotranspiration or sublimation infiltrates the soil. If the pore space of the top soil is suffused and the hydrologic input surplus is greater than the recharge to the subsoil, water will be lost as overland flow. Water that is not lost to surface runoff will eventually recharge the aquifer. Once in the aquifer, all water exits the coastline as fresh SGD. In reality, some meteoric groundwater may discharge above mean sea level as near-shore terrestrial groundwater discharge (NGD; Luijendijk et al., 2020). Our calculations provide fresh SGD and NGD as one combined term, which we will continue to term fresh SGD (Figure 1). Coastal aquifers are further partitioned into five main lithologic classes derived from regional geologic maps to apply necessary aquifer parameters from Gleeson et al. (2014) and to assess relative contributions from each class. In the absence of suitable hydrogeologic datasets for the region, both models rely on regional and global datasets to assign hydrologic, geologic, soil, and aquifer inputs and parameters to each coastal catchment. Interbasin flow, water originating from outside the catchment boundaries, is neglected. The results present fresh SGD estimates as volumes of water per time that a coastal catchment discharges to the ocean.

3.2 Model Structure, Forcing, and Flux Calculation

3.2.1 Lumped Parameter Coastal Catchment Regional Fresh SGD Model

The first approach applies a lumped parameter regional model (LPRM) modified from Hajati et al. (2019) and accounts for water volumes of the top soil $S_1(t)$ (mm), sub soil $S_2(t)$ (mm), and the aquifer $S_3(t)$ (mm) to represent the main processes of soil and aquifer interactions therein. Hajati et al. (2019) validated their model results with averaged groundwater flows from seven globally available models. They found that their model predicts similar groundwater fluxes to those from the global model results, with the majority of catchments falling within the calculated range. Our implementation of the model is tested using the same input from Hajati et al. (2019), which provided model results with minimal variation from the original work.

Output for the LPRM is performed at a daily timestep, t, which corresponds to the resolution of the hydrologic input data. The water balance for the top soil for each coastal catchment of the GoA drainage basin is given by:

$$\frac{dS_1}{dt} = P + M + CR - (ET + SU) - OF - R_1 \quad (1)$$

where S_1 is the volume of water stored in the catchment topsoil, and the precipitation input P, snow- and ice-melt input M, capillary rise to the top soil CR, evapotranspiration ET, snow sublimation SU, surface runoff OF, and subsoil recharge R_1 are all taken in rate form (mm/day). The top soil is separated from the aquifer by the sub soil. The water balance for the sub soil S_2 is given by:

$$\frac{dS_2}{dt} = R_1 - CR - R_2 \quad (2)$$

where aquifer recharge R_2 is taken to be in rate form. The aquifer is represented by the last reservoir, which has no maximum storage threshold. The water balance for the aquifer is given by:

$$\frac{dS_3}{dt} = R_2 - SGD \quad (3)$$

where fresh SGD is taken to be in rate form. The model compares the stored water in the aquifer reservoir on the final day of the model run (31 August 2014) with the first day (1 September 1979) and ends the model spin up if those aquifer levels are within 1 mm of each other. This results in high variability for the number of model runs it takes to reach a water balance in each catchment.

The initiating step fills up the top soil with precipitation and meltwater and then reduces the water content via evapotranspiration and sublimation from snow. Rather than repeating computationally expensive physically based water and energy balance models for this input, our study leverages an existing hydrological model for the GoA (GoA HM; Beamer et al., 2016) that solves for the required input. Beamer et al. (2016) provide high spatial and temporal resolution (1 km x 1 km; daily time step) discharge data for the entire domain. The GoA HM uses a collection of physically based models that drive runoff to 14,052 discharge outlets. Meteorological forcings are interpolated to the resolution of the elevation and land cover data (MicroMet; Liston and Elder, 2006a), runoff from rainfall and the full evolution of the snow water equivalent from snow and ice are calculated (SnowModel; Liston and Elder, 2006b) along with actual evapotranspiration, surface and baseflow runoff (SoilBal; Beamer et al., 2016), and runoff is routed from cell to cell, down-gradient (HydroFlow; Liston and Mernild, 2012). The GoA HM lumps all freshwater discharging to the ocean into a singular runoff term and does not distinguish stream discharge from groundwater discharge. For this study, we assume that the discharge outlet of the GoA HM represents the net hydrologic forcings of a coastal catchment for one day and we redistribute that value over each coastal catchment to perform the water balance. This assumption is valid for the small control areas we use for our coastal catchments since water traveling over such short, steep drainage lengths typically takes much less time than the timestep at which the model is forced. By using the GoA HM as input, we may reduce the water balance for the top soil to:

$$\frac{dS_1}{dt} = HI_{net} + CR - OF - R_1 \tag{4}$$

where the net hydrologic input HI_{net} is also in rate form.

Surface flow is generated if the water content of the top soil exceeds the input in the first step:

$$OF(t) = \begin{cases} 0 & if\ S_1(t) \leq S_{max,1} \\ S_1(t) - S_{max,1} & if\ S_1(t) > S_{max,1} \end{cases} \tag{5}$$

where $S_{max,1}$ is the maximum available water volume of the top soil. This parameter is supplied by the Global Land Cover Characteristics database (Loveland et al., 2000), which delineates the global surface into 99 classes, each of which are given water-holding capacities W_{ava} (mm) by Hagemann (2002).

The following step sees a reduction in the water content of the top soil through sub soil recharge $R_1(t)$. The pressure head h necessary to calculate the unsaturated hydraulic conductivity is calculated using the effective saturation Θ by:

$$\Theta(\mathrm{t}) = \frac{\theta_1(t) - \theta_{res}}{\theta_{sat} - \theta_{res}} = (1 + (\alpha\ _1)^{N_1})^{-m_1} \quad (6)$$

where θ_{sat} (mm) and θ_{res} (mm) are saturated and residual contents, respectively, and α_1 (mm^{-1}), N_1, and $m_1 = 1\text{-}1/N_1$ are top soil van Genuchten curve-fitting parameters that are empirically derived to describe soil water retention curves (Van Genuchten, 1980). The α parameter in this model is related to the inverse of the air entry suction while the N parameter is the measure of the pore size distribution. The water content of the reservoir $\theta(t)$ is the volume of water within the reservoir $S_1(t)$ divided by the total volume of the reservoir V_{tot}, where $V_{tot} = S_{max} / \varepsilon_1$ and $\varepsilon_1 = \theta_{sat} - \theta_{res}$. For both the top soil and sub soil reservoirs, N, α, θ_{sat}, θ_{res}, and saturated hydraulic conductivity K_{sat} (cm/day) are provided by the HiHydroSoil v2.0 data set at a resolution of 250 m worldwide (Simons et al., 2020). This data set gives values for the top soil and sub soil at 0 to 0.3 m and 0.3 to 2.0 m depth, respectively. Recharge to the sub soil $R_1(t)$ is equal to the unsaturated hydraulic conductivity $K_{unsat}(t)$ of the top soil given by (Van Genuchten, 1980):

$$K_{unsat,1} = K_{sat,1} \frac{[1 - (\alpha_1 h_1(t))^{N_1 - 1}[1 + (\alpha_1 h_1(t))^{N_1}]^{-m_1}]^2}{[1 + (\alpha_1 h_1(t))^{N_1}]^{m_1/2}} \quad (7)$$

The water lost from the top soil via recharge R_1 is added to the sub soil. If the sub soil is full, the excess water is added back to the topsoil. If this results in filling up the top soil, additional

surface runoff $OF(t)$ is generated. Additionally, the sub soil loses water to the top soil via capillary rise $CR(t)$ by:

$$CR(t) = K_{sat,2}(t) \cdot \left(\frac{S_1(t)}{S_{max,1}}\right) \quad (8)$$

Greater amounts of water are transported to the top soil when water content is lower within the top soil. Again, if this generates excess water within the top soil $S_1(t)$ it is added to surface runoff $OF(t)$.

The sub soil loses water to the aquifer reservoir via recharge $R_2(t)$, which is equal to the unsaturated hydraulic conductivity of the sub soil $K_{unsat,2}$ (Equation 7). This water then exits the aquifer as fresh SGD which is equal to the storage volume within the aquifer $S_3(t)$ multiplied by the recession parameter R_3 as defined by (Kraijenhoff Van de Leur (1958)):

$$R_3 = \frac{\pi^2 K_{sat,3} D_3}{\varepsilon_3 L^2} \quad (9)$$

where $K_{sat,3}$ is the saturated hydraulic conductivity of the aquifer (mm/day), D_3 is the aquifer thickness (mm), ε_3 is the aquifer porosity, and L is drainage width of the aquifer (mm). Coastal catchments are divided into five main lithologic classes as determined by the dominant rock type within each catchment from the Geologic Map of Alaska (Wilson and Labay, 2016). Gleeson et al. (2014) assign porosity and permeability values for each lithologic class, which are then converted to saturated hydraulic conductivity (Kozeny, 1927) using standard values for water at 20 °C. D_3 is provided by the global 1-km gridded thickness of soil, regolith, and sedimentary deposit layers data set from Pelletier et al. (2016). Top soil and sub soil thickness are subtracted from these provided values to determine the thickness of the aquifer layer, which is >5 m. Assuming a roughly triangular shape for each coastal catchment, the average groundwater flow width L is half the orthogonal distance between the furthest inland point and the coastline (Van de Leur, 1958).

Model parameters are extracted for each coastal catchment using ~~custom~~ workflows in ArcGIS Pro 3.0.2. A complete list of the data necessary for the model input is provided in Table S1. Aside from the vectorized geologic map, all of the input variables for this model are available in raster format. Due to the spatial location of coastal catchments, which are on continental margins, the available raster data often has incomplete or missing coverage over their domain since these data represent continental features. We expand the coverage of these data sets by performing focal statistics over a 3x3 rectangular neighborhood where the mean value is applied to center of that neighborhood. We avoid altering the original dataset by mosaicking the original raster to the newly generated raster, which uses the original raster as the preferred mosaic operator. This is performed a maximum of four times for each model parameter which allows for a more complete coverage over coastal catchment domains. Model parameters are then extracted for each coastal catchment using zonal statistics, which applies mean values to each.

Geologic units provided by the USGS Geologic Map of Alaska (Wilson and Labay, 2016) are grouped into five main lithologic classes to apply aquifer permeability and porosity for each class from Gleeson et al. (2014). We extract the dominant rock type for each coastal catchment using standard GIS techniques. Gleeson et al. (2014) provides sublithologies that account for grain size for both unconsolidated and silicious sedimentary units. We assume that coastal catchments composed of unconsolidated deposits have permeability and porosity values associated with coarse-grained sediments. We consider this to be a valid assumption in the mostly high-energy depositional environments in which these sediments are deposited. Further, the effective permeability is more likely to reflect the most permeable sub-unit in layered unconsolidated deposits. We also choose not to separate silicious sedimentary units based on grain size. Although much of the sedimentary geology along the GoA is dominated by fine-grained units such as shale, these units are also highly fractured, shifting the associated permeability and porosity towards those observed in coarse-grained deposits. Thusly, we use median values for siliceous sedimentary hydrolithologies to describe this unit.

Table 2. Summary of number, averaged catchment properties, averaged hydrologic input, and averaged model parameters for coastal catchments separated by main lithologic classes

	Catchment Properties			Hydrologic Input		Input Parameter					
Lithology	Count	Area [km^2]	GW flow width [m]	Beamer et al. (2016) [mm/yr]	GLDAS (avg.) [mm/yr]	$K_{sat,1}$ [mm/day]	$K_{sat,2}$ [mm/day]	$K_{sat,3}$ [mm/day]	$S_{max,1}$ [mm]	$S_{max,2}$ [mm]	D_3 [m]
C.g. unconsolidated	2200	3.5	1075	2454	526	275.5	171.1	10671	206.9	369.4	18.4
Sil. sedimentary	5855	2.9	859	3070	643	499.1	138.6	1	195.1	374.2	4.9
Crystalline	3608	2.9	855	3265	810	190.4	134.9	7	195.1	372.6	5.0
Volcanic	819	3.0	841	3020	816	159.4	107.1	268	192.4	373.3	5.7
Carbonate	414	2.5	668	3592	827	145.4	90.5	1343	180.9	370.1	6.0
Model Domain	12896	3.0	887	3033	687	206.8	139.2	1883	196.5	372.7	7.3

Partitioned by geology, coastal catchments composed of unconsolidated deposits contain the largest averaged areas and groundwater flow widths, while carbonate coastal catchments contain the smallest (Table 2). The highest averaged saturated hydraulic conductivities of the top soil are observed in silicious sedimentary environments, whereas the highest averaged saturated conductivities of the subsoil and aquifer containers are seen in unconsolidated deposits. Maximum averaged storage volumes of the topsoil are also recognized in unconsolidated deposits, along with the largest averaged aquifer thickness, while the subsoil has a similar maximum averaged storage volume across lithologic classes (Table 2).

3.2.2 Global land surface models water budget approach

Fresh SGD is also estimated using the simple water budget approach from Sawyer et al. (2016), and Zhou et al. (2018, 2019). This method uses the same coastal catchment recharge areas as described previously. Recharge across these coastal catchments is the surplus of precipitation and meltwater that infiltrates the surface. This recharge would eventually discharge to a stream if one were present, but by isolating coastal catchments as areas lacking streams, we may assume that all recharge to these systems eventually discharges to the coast as fresh SGD. We assume a small net imbalance between groundwater injections and withdrawals, which is very reasonable in such a remote and sparsely populated landscape. We also assume that the net imbalance

between the import and export of groundwater between catchments, or interbasin flow, is negligible. Under long-term steady state conditions, these assumptions allow the calculation for annual volumes of fresh SGD to simply be the linear average net recharge r integrated across coastal catchment areas A (Zhou et al., 2018):

$$Q_{freshSGD} = r \cdot A \quad (10)$$

where $Q_{freshSGD}$ and r are in rate form. The calculation may also be made as annual volumes of fresh SGD per unit length in coastline by:

$$Q_{freshSGD} = \frac{(r \cdot A)}{CL} \quad (11)$$

where CL is the coast length for each coastal catchment.

We use values calculated from two global land surface models provided by NASA's Global Land Data Assimilation System (GLDAS, Rodell et al., 2004) to approximate the average net recharge rate for each coastal catchment. There are three land surface models currently driven by GLDAS: NOAH, Catchment (CLSM), and the Variable Infiltration Capacity (VIC). All three aim to generate variables of states and fluxes occurring at the land surface using advanced modeling and data assimilation techniques (Rodell et al., 2004). Although there are three components to GLDAS, our study relies exclusively on GLDAS-2.0 which is the sole option that supplies a temporally consistent time series during our historical model period (1 September 1979 through 31 August 2014). Doing so allows for intermodel comparisons with our approach in the previous section. The simulations of GLDAS 2.0 are forced by Princeton meteorologic input data to drive model outputs (Sheffield et al., 2006). The three land surface models provide data products that contain 34-38 output parameters. One of these parameters is baseflow-groundwater runoff (kg/m^2/t), which is what we use to generate our recharge term for the coastal catchment domains (equation (10)). The models do not explicitly solve for lateral groundwater

flow, but rather provide a one-dimensional vertical component for groundwater runoff. Conceptually this is similar enough to groundwater recharge as it solves for the flux of water from the surface to deeper components of the soil. We only apply data products from NOAH and CLSM as they are provided at a higher spatial resolution (0.25° x 0.25°) than those from VIC (1.0° x 1.0°).

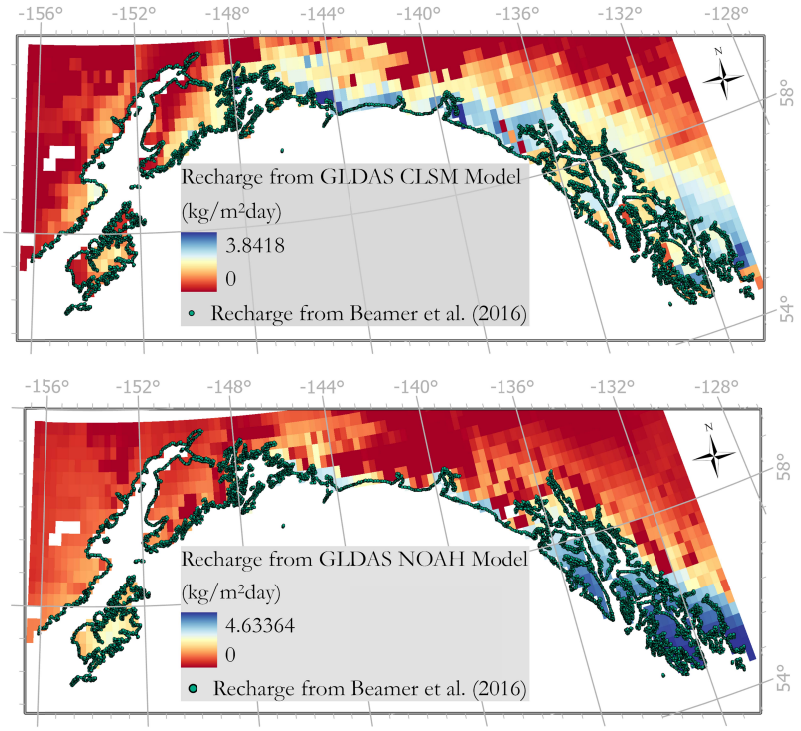

Figure 3. Baseflow-groundwater runoff along the GoA margin from CLSM (top) and NOAH (bottom) data products used in our calculations for annual volumes of fresh SGD. The net hydrologic input for each coastal catchment in our method in the previous section are displayed as green circles.

The baseflow-groundwater runoff data product from the NOAH and CLSM land surface models are accessed through NASA's Giovanni online web environment (Acker and Leptoukh, 2007). We averaged the data product timeseries for each pixel over the domain of our model for both NOAH and CLSM. Coastal catchments are assigned recharge rates from both models by extracting values from the pixel with the closest centroid to each catchment. This approach is valid for our purposes since all of the coastal catchments are significantly smaller than the

GLDAS data products resolution ($\leq 20km^2$ vs. 0.25°). The extraction of NOAH and CLSM data products resulted in the 12,896 coastal catchments along the GoA being represented by 319 and 321 pixels, respectively. This is much less than the input used in the previous method, which has a unique net hydrologic input for each individual catchment (Figure 3). Data products are multiplied by the catchment area (equation (10)) and converted to annual volume rates of fresh SGD for each coastal catchment. We average the two results to compare with our previous approach.

4 Results

4.1 Lumped Parameter Regional Model (LPRM) Estimates

Along the coastal margin of the GoA, 12,896 coastal catchments generate a mean fresh SGD flux of 86.8 km^3/yr, or 11.4% of the total freshwater discharge (FWD) as provided by Beamer et al. (2016). Integrated over the 28,069 km of coastline, the total contributing recharge area of these coastal catchments is 38,650 km^2, or 9.2% of the entire drainage basin. The average stretch of the GoA shoreline offers 8.47 m^3/day per meter of coast of fresh SGD, which is just under 1 cm^3/second. While the total daily freshwater discharge varies considerably over the course of a year, daily fresh SGD remains relatively sustained (Figure 4). Over the 35-year period of our model run, total daily fresh SGD never drops below 0.23 km^3/day, which is only 4.7% off from the mean daily value of 0.241 km^3/day. Peak daily fresh SGD observed in any given year is not far off from the lowest yearly contributions, whereas FWD approaches zero at the beginning of each calendar year and has an annual variability that consistently spans over two orders of magnitude. Additionally, the highest fresh SGD peaks over the course of the model period do not coincide with peaks observed in total freshwater discharge. This indicates that fresh SGD to the GoA may be a sustaining contribution with respect to both freshwater and nutrient delivery regardless of season, as well as during relatively low flow years.

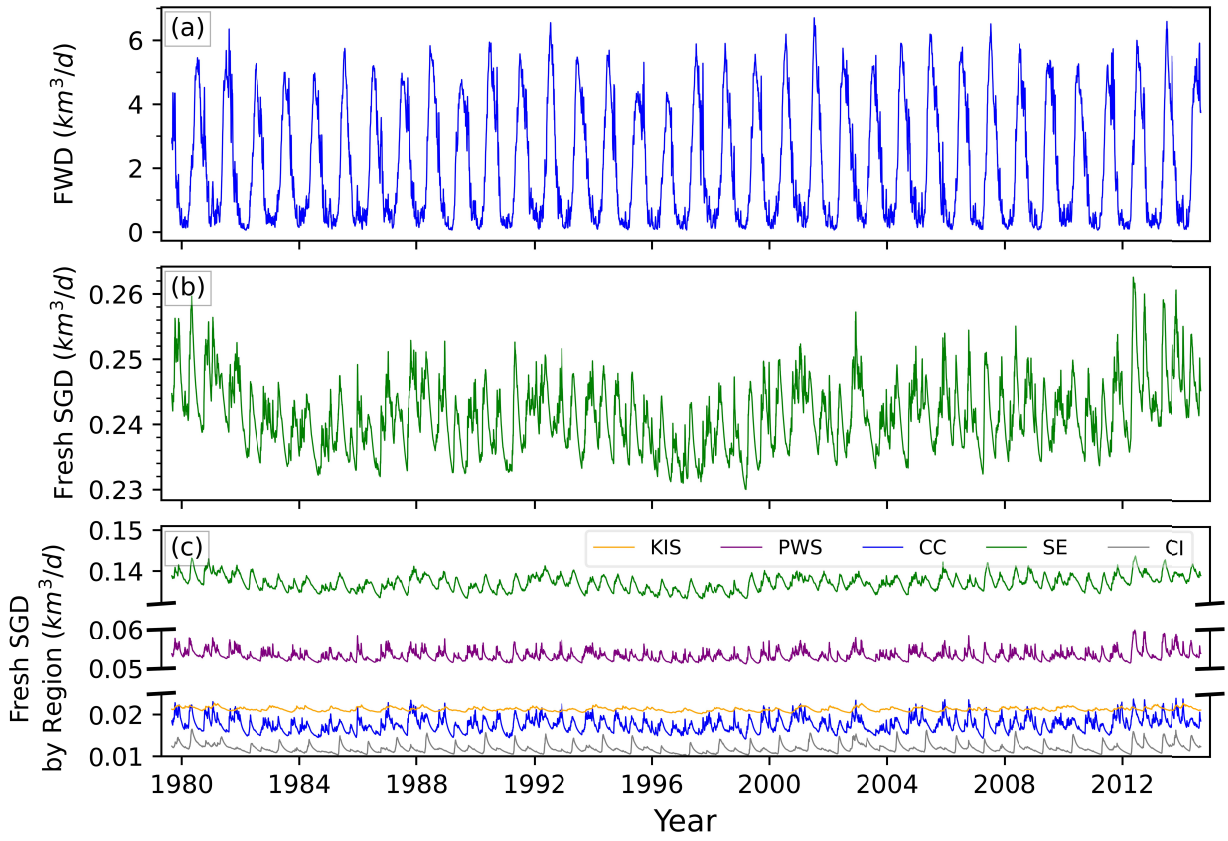

Figure 4. Multidecadal trends in daily modeled freshwater discharge (FWD) and fresh submarine groundwater discharge (SGD) to the Gulf of Alaska. (a) Daily modeled total freshwater discharge from Beamer et al. (2016); (b) daily modeled fresh SGD from the lumped parameter regional model approach; (c) fresh SGD broken down by subregion. Subregions, from west to east, are Kodiak Island/Shelikof (KIS), Cook Inlet (CI), Prince William Sound (PWS), Central Coast (CC), and Southeast (SE).

Fresh SGD is highly variable throughout the region, with the highest input from the Southeast subregion, and the lowest input occurring in the Cook Inlet basin (Figure 4). Basin wide median peak daily fresh SGD flux occurs during the month of May, while the lowest median daily values occur in August (Figure S1). This observation holds true for the Cook Inlet and Southeast subregions, however, this is not characteristic for the Kodiak Island/Shelikof, Prince William Sound, and Central Coast. The Prince William Sound and Central Coast subregions reach a median daily maxima during the month of October, while peak median values for Kodiak Island/Shelikof occur in January. This suggests that the coastal catchments within these

560 subregions receive much of their recharge from fall and winter rains, whereas the basin as a
561 whole achieves peak discharge due to snow melt. Dissimilarly, total daily FWD is relatively low
562 during the winter months, reaching a minima during the month of February. This is six months
563 from the median daily minima for total fresh SGD, and also occurs during a time where mean
564 values of fresh SGD exist. Over the model period, total daily fresh SGD reached a maximum
565 contribution of 0.273 km^3 in May of 2012.
566
567 The spatial variability of fresh SGD along the GoA margin depends on both the contributing area
568 of coastal catchments and the water availability necessary to recharge the coastal aquifers. In the
569 top panel of Figure 5, annual fresh SGD volumes and coastal catchment area are grouped into
570 0.1° longitudinal bins and smoothed to observe trends along the shoreline. Both coastal
571 catchment area and discharge achieve a broad peak in the east, providing a premise for why the
572 overwhelming majority of fresh SGD results from the Southeast subregion. Moving to the west,
573 coastal catchment area falls dramatically until reaching the Prince William Sound, apart from a
574 small increase seen in Yakutat Bay. Both coastal catchment area and fresh SGD increase
575 substantially within the Prince William Sound, effectuating the greatest specific discharge, or
576 discharge normalized by recharge area, observed along the coastline. To the contrary, the lowest
577 specific discharge is observed in the Cook Inlet and Kodiak Island/Shelikof subregions when
578 moving to the west. Coastal catchment area remains relatively similar to the areas observed
579 within the Prince William Sound, suggesting that water availability is the stronger driver of fresh
580 SGD in these regions. On the other hand, the high density of coastal catchments areas in the
581 Southeast and Prince William Sound subregions are a strong driver of fresh SGD volumes. This
582 offers an insight that high-latitude island chains and archipelagos may disproportionately
583 contribute to the overall fresh SGD flux. We provide a map of fresh SGD hotspots along the
584 GoA margin derived from the LPRM approach in Figure 5.

585

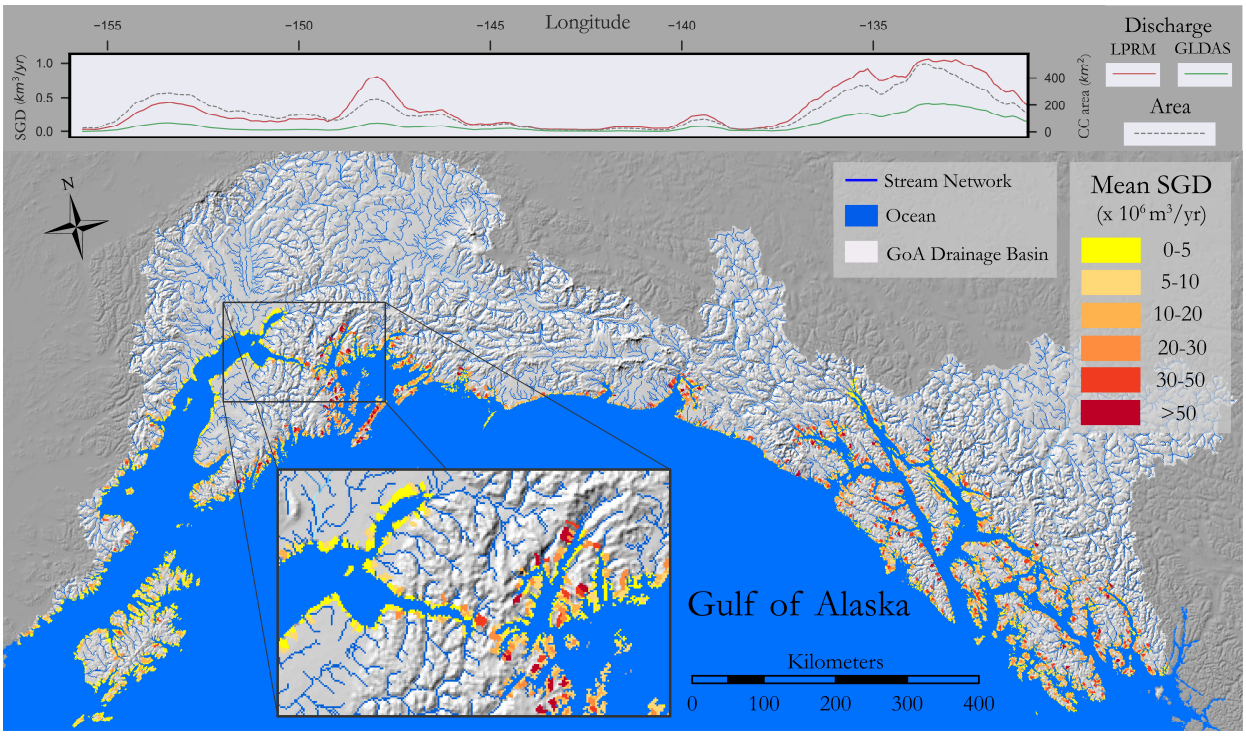

586

587 **Figure 5**. Map of mean annual fresh submarine groundwater discharge volumes from the lumped
588 parameter regional model (LPRM) along the Gulf of Alaska coastline. Fresh submarine
589 groundwater discharge from the LPRM (red) and GLDAS (green) are plotted with coastal
590 catchment area as a function of longitude along the top of the map. The inset map corresponds to
591 subregions with the lowest (left side) and highest (right side) specific discharges. The stream
592 network of the GoA is depicted as blue lines and the Gulf of Alaska drainage basin is highlighted
593 in light grey.

594

595 ## 4.2 GLDAS Water Budget Estimates

596

597 The water budget approach using GLDAS data products for the recharge input predicted a total
598 mean annual fresh SGD volume of 26.5 km^3. This is about one third less than those estimated
599 from the LPRM method, and represents 3.5% of the total FWD to the GoA (Table 3). This
600 contribution is the average from the values derived using the two discrete inputs from the CLSM
601 and NOAH land surface models. Results between the two inputs are typically within a factor of

602 two of each other. The estimates using the CLSM data products generally provide lower
603 estimates than those from NOAH, with total mean annual contributions of 18.9 km^3 and 34.0
604 km^3, respectively. Estimates using CLSM products as inputs do provide higher input than those
605 from NOAH for some coastal catchments within the PWS and CC subregions. Averaged
606 between the two, the mean daily input of fresh SGD per meter of coastline is 3.3 m^3, or 0.4
607 cm^3/s.
608

609 **Table 3.** Annual fresh SGD results across methods.

610

Hydro-climate data	Model	Mean fresh SGD flux (m^2/year)	Median fresh SGD flux (m^2/year)	Total fresh SGD (km^3/year)
GLDAS	Water Budget-NOAH v2.0	1,543.1	767.1	34.0
	Water Budget-CLSM v2.2	864.9	432.9	18.9
	Average:	1,204.0	600.0	26.5
Beamer et al. (2016)	Lumped Parameter Regional Model:	4,091.3	2,541.3	86.8

611

612 Spatial variability of annual mean fresh SGD using GLDAS data products show similar patterns
613 across the GoA landscape to the estimates obtained from the LPRM approach. The top panel of
614 Figure 5 presents fresh SGD volumes as a function of longitude for the averaged results from
615 GLDAS data products in green. Coastal catchment recharge areas are held constant between both
616 estimation methods. The greatest input of fresh annual SGD is observed with the same
617 distinctive broad peak over the SE subregion. Similar peaks are also recognized within the center
618 of the CC and across the PWS. The lowest contributions are found in the western portion of the
619 CC.
620

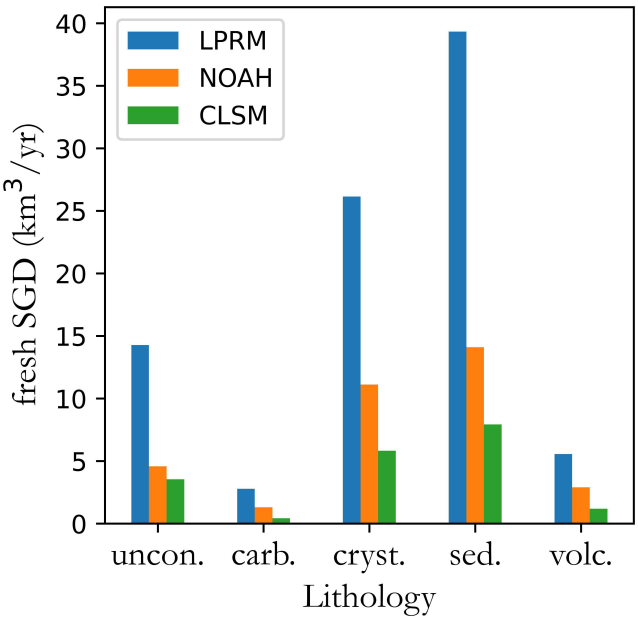

Figure 6. Mean annual fresh SGD results from multiple methods, separated by lithologic mediums. Abbreviations are for unconsolidated deposits (uncon.), carbonate (carb.), crystalline (cryst.), siliceous sedimentary (sed.), and volcanic (volc.).

This method also results in similar patterns to those of the LPRM when discharge volumes are parsed by coastal catchment lithology. This may benefit future analyses that estimate the geochemical contribution of groundwaters across the region. The overwhelming majority of fresh SGD is sourced from catchments dominated by siliceous sedimentary rock units, while the lowest contribution discharges from carbonate geology (Figure 6). This is expected when considering the occurrence of these lithologies over this predominately rocky coastline, where sedimentary and carbonate units constitute around 44% and 2.7% of the coastal catchment domains, respectively. Sedimentary catchments also have a much higher average top soil saturated hydraulic conductivity $K_{sat,1}$ than other lithologies (Table 2). On the other hand, the aquifers of sedimentary catchments have the lowest saturated hydraulic conductivity, allowing the media more influence over the constituents of freshwater (Table 2). Catchments composed of unconsolidated deposits have the lowest area normalized fresh SGD contribution. A major portion of these deposits are located in the CI basin, which has a lower water availability when compared to the rest of the region. Annual fresh SGD volumes using CLSM and NOAH data

640 products as inputs are most similar within these unconsolidated catchments, and have the greatest
641 difference within carbonate catchments (Figure 6).
642

643 **5 Discussion**

644 5.1 Comparison of approach

645

646 Fresh SGD flux estimates over this expansive region are relatively consistent considering the
647 complex landscape and hydrology of the domain. Both methods provide results with comparable
648 assumptions and limitations, as well as benefits for each. Our annual flux estimates all agree
649 within a factor of 2.5 to 5 when summed over the entire coastline, regardless of differences
650 between the hydrologic input data or computational method. At the catchment-scale, agreement
651 between the approaches is highly variable with only 3% of 12,896 coastal catchments falling
652 within a range of ±50% of one another (Figure 7a). The LPRM approach yields consistently
653 higher fresh SGD rates for the majority of cases. This is likely due to the coarse resolution used
654 by the GLDAS results which may be more representative of dryer, continental domains. Even so,
655 catchment-specific estimates are well within an order of magnitude from one another when
656 catchments with zero discharge from GLDAS inputs are excluded. This is an acceptable range
657 given that global estimates range over about three orders of magnitude, or from approximately
658 0.1 to 10% of river flow (Taniguchi et al., 2002). Both models also highlight the importance of
659 smaller catchments distributed throughout the model domain. In Figure 7b, coastal catchments
660 are ordered from smallest to largest to assess the relative contribution of fresh SGD based on
661 contributing area. The majority of fresh SGD proceeds from coastal catchments that are less than
662 5 km^2 in area, even more so in the LPRM approach than from the water budget using GLDAS
663 inputs.
664

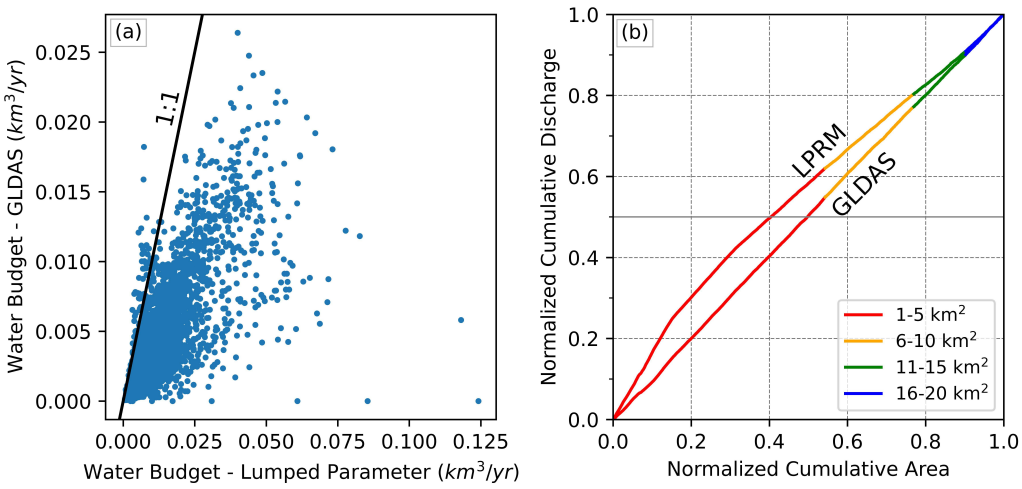

Figure 7. Comparison plots of modeled fresh SGD across the GoA. (a) Cross plot of modeled fresh SGD flux for each catchment using different methods to estimate flux; (b) Plot showing the distribution of fresh SGD by coastal catchment area ordered from smallest to largest for each method. Line segment colors correspond to a 5 km^2 range of contributing recharge area, normalized by the total area of coastal catchments, plotted against the cumulative sum of discharge volume normalized by the total SGD volumetric flux for each method.

The major benefit of using GLDAS data products in a water balance approach is that the recharge term has already been solved for by multiple global land surface models. This greatly reduces the computational time and effort for estimating fresh SGD over large regional or global domains. Further, the recent availability of web based applications, such as Giovanni, allows for the condensation of data discovery, query, manipulation, visualization, and download into one fluid process. This efficiency comes at the cost of spatial resolution, which may misrepresent the site specific processes occurring within our significantly smaller domain boundaries. Discharge from individual coastal catchments may be more representative of those from larger, more inland tracts of land, which typically acquire decreased hydrologic input when compared to coastal areas in the GoA (Bieniek et al., 2014). Additionally, fresh SGD fluxes from GLDAS are more consistent than those from the LPRM estimates that use high-resolution hydrologic input. This diminished variability is due to the coarser resolution (0.25° x 0.25°) of the GLDAS data products, which represent all 12,896 coastal catchments with only 319-321 pixels (Figure 3). GLDAS data products have modeled some of the pixels within our domain as having zero

687 recharge, likely due to the majority of the cell being occupied by ice. The occurrence of these
688 cells is highly variable between the NOAH and CLSM data products, especially within the PWS
689 and CC subregions (Figure 3). A relatively small portion of these coastal catchments contain
690 glaciers, and the catchments that are included are primarily representative of the appointed
691 lithologies from which they drain to the coast. This has led to further catchment-scale
692 discrepancies between our model results, particularly in areas with partial ice cover (Figure 7a).
693
694 The LPRM approach requires the discovery, acquisition, and download of multiple datasets
695 before extensive manual preprocessing operations may initiate. This results in notably larger file
696 sizes that effect storage, handling, and processing during modeling operations that are markedly
697 more computationally expensive. A model run-time of over 216 hours is required for fresh SGD
698 model results to reach a water balance for the 12,896 coastal catchments along the GoA, despite
699 applying parallel processing practices that initiate the use of all sixteen cores on our processor
700 for parsed model bins. However, there are several advantages associated with this increased
701 computational expenditure. First, each individual coastal catchment may be uniquely represented
702 by higher resolution hydrologic input and soil parameters. This finer degree is important in the
703 assessment of localized contribution and variability, especially if the results are to be compared
704 with local-scale studies in the future. Additionally, model results may achieve the temporal
705 resolution of their required hydrologic input. This allows for an in-depth analysis of time-series
706 results across periods of interest. This is particularly important when characterizing fresh SGD,
707 for this flux has been shown to demonstrate a high degree of seasonality (Michael et al., 2005).
708 Finally, the LPRM model provides results for each component of the water balance at the
709 catchment-scale, allowing for localized assessment of the relationships between catchment-
710 specific properties and inputs and the resulting flux over both time and space (Figure 8). GLDAS
711 models solve for a myriad of components of the water cycle, most of which are not very useful
712 for the domain of this study. For example, the GLDAS surface runoff data product includes
713 watersheds that house large river systems, which is much less representative to our coastal
714 catchments than the recharge term. Furthermore, recharge and fresh SGD are solved separately,
715 whereas they are assumed to be the same in the other approach.
716
717

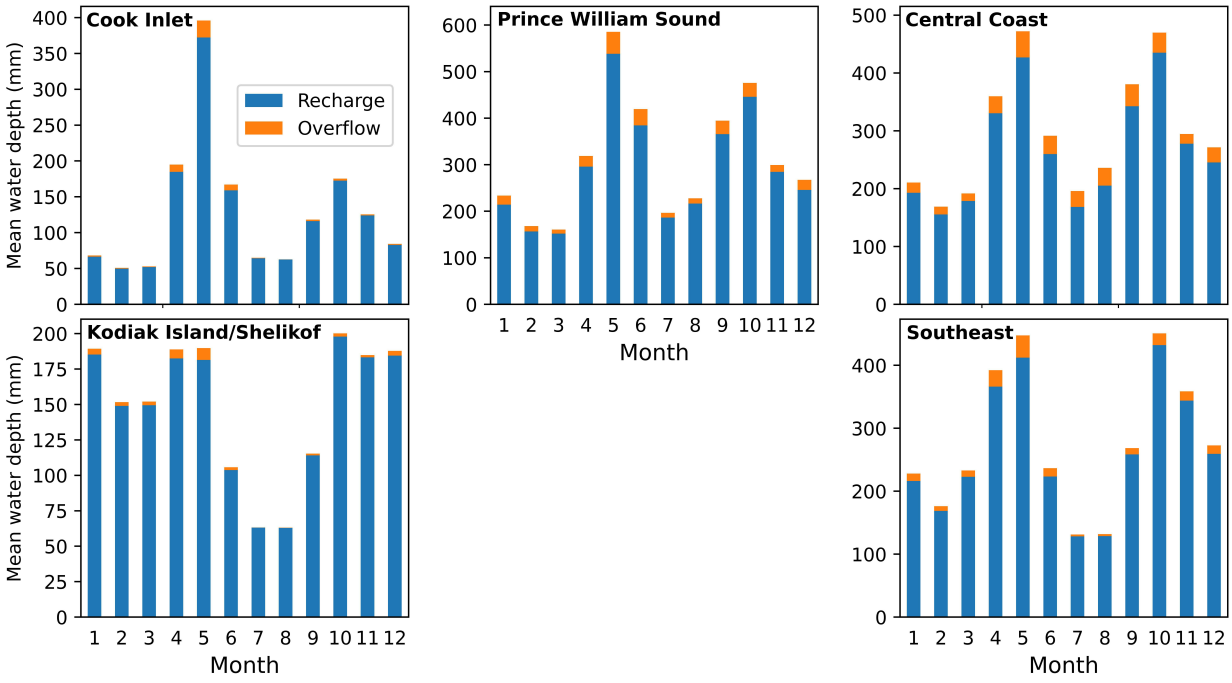

Figure 8. Stacked plots of mean monthly aquifer recharge, R_2, and overflow, *OF,* normalized by area. Values are calculated from the lumped parameter regional model results and are representative of the mean water depths across all catchments within a subregion.

5.2 Current limitations in the water balance approach

The different conceptualizations of coastal aquifer dynamics we explore provide a simple means to estimate fresh SGD over large regional scales. Currently, there are several processes that must be incorporated into future approaches to allow for a better representation of these systems. This is especially true for the dynamic coastline of the GoA. In both approaches, recharge to these systems is assumed to occur solely within topographically defined boundaries of individual coastal catchments and does not consider interbasin flow from adjacent watersheds. This may substantially underestimate fresh SGD in the region, especially within unconsolidated coastal catchments that are part of a larger glacial-fluvial outwash plain containing large meltwater streams. Coastal catchments on the peripheries of these predominately coarse deposits potentially source a large portion of their recharge from their streams, though limited research has explored the magnitude of this flux. Mackay et al. (2020) estimated a meltwater river to contribute 13-17% of the total aquifer recharge in a proglacial sandur of Iceland. Concentrated infiltration has

been observed elsewhere as an important agent of groundwater recharge in proglacial environments, even within the GoA drainage basin (Liljedahl et al., 2017; Ó Dochartaigh et al., 2019; Somers and McKenzie, 2020). Further, groundwater flow occurs through the full thickness of the materials within these infilled valleys and plains occupied by meltwater streams. Fresh SGD is likely amplified in these environments, where groundwater discharges parallel to the mouths of rivers to the coast (Yu et al., 2021). In geologic analogues, groundwater flow through a proglacial unconfined aquifer is estimated to be 9.8% of the mean annual river flow if the full thickness is considered (Ó Dochartaigh et al., 2019). This is not only likely to underestimate the fresh SGD estimates, but may have resounding implications for the total freshwater discharge delivered to the GoA. Phelan Creek, one of the sites used for calibration in the GoA RM (Beamer et al., 2016), was recently observed to lose potentially half of its annual streamflow to groundwater (Liljedahl et al., 2017). Like Phelan Creek, the majority of gauging sites within the region are located on thick, extensively filled valleys where subsurface flow is not quantified. Additional sources of fresh SGD may result from sub-glacial groundwater recharge (Boulton and Caban, 1995; He et al., 2022) or in larger watersheds that contain ephemeral or intermittent streams.

While water balances provide a simple means to estimate the contribution of the fresh SGD flux, groundwater flow is governed by physically-based processes. The water balance approach is unable to resolve effects that may result from aquifer heterogeneity or dual-density flow, both of which are inherent to these systems (Robinson et al., 2018). The two approaches we incorporate into our estimates have both been compared with other external data sets. Zhou et al. (2018) compared the water balance approach to numerical flow models over the same region in the Atlantic and Gulf Coast regions of the conterminous United States. They found agreeance between water budget and numerical modeling approaches to be within a factor of 2 to 3 when fluxes are summed over the entire coastline. Hajati et al. (2019) compared their fresh SGD results from the Island of Java using the LPRM approach with global groundwater model results, most of which solve a water balance that is conceptually and methodically similar to GLDAS. The comparison highlighted discrepancies that ranged over three orders of magnitude between the LPRM results and those from global models. Further, the authors found no clear correlations of daily fresh SGD and the four categories chosen for their sensitivity analyses. In the absence of

local and regional numerical flow models or in-situ studies concerning fresh SGD within the GoA, we chose to focus our analysis on the comparison between two previously applied water balance approaches that may be validated against future studies.

5.3 A call for localized research on fresh SGD within the GoA and similar high latitude environments

This study focuses on fresh SGD to the GoA due to its disproportionate importance concerning global scale hydrology. The magnitude of fresh SGD and its influence remains virtually unexplored within high-latitude active margins globally. Our model results highlight the potential significance of fresh SGD to the GoA and the coastal communities and ecosystems therein. Although fresh SGD is estimated to be substantially lower than the total FWD volumetrically, the enriched nutrient and solute concentrations observed within these coastal aquifers globally could make it a powerful influencer on near-shore marine ecosystems in the region. The GoA system is undergoing climate mediated alterations at a rapid pace, and understanding how coastal groundwater systems are responding is not currently a part of this conversation. Improvements in remote sensing, in-situ data collection, and computing are facilitating readily available opportunities to estimate fresh SGD over a range of spatial scales within the GoA. Here we provide a regional estimate, but understanding local-scale hydrologic feedbacks and contributions is critical to develop a complete understanding of nutrient, solute, and freshwater transport within the region, and how they are changing with accelerated warming. Further, the state of Alaska is markedly lacking in subsurface observations, such as hydraulic head, critical to calibrate and validate groundwater flow models for the region.

6 Conclusion

This study is the first to estimate the regional contribution of fresh SGD to the GoA. We supply estimates from two accepted water balance approaches and compare the results. Our findings suggest that fresh SGD along the coast is a significant source of freshwater to the GoA, contributing between 3.5-11.4% of the total freshwater discharge, depending on the method applied. Further, we highlight fresh SGD as a sustained delivery of freshwater and nutrients to the coast, even during relatively low surface water discharge years. Both methods of approach result with an agreement between a factor of 2.5 and 5 when summed along the entire coastline.

The spatial distribution of fresh SGD is largely dependent on regional water availability and the occurrence of recharge areas, with notably more contribution resulting from areas with abundant islands and archipelagos. The majority of fresh SGD flows from catchments predominately composed of siliceous sedimentary lithology. The highest and lowest specific discharge occur in the Prince William Sound and the Cook Inlet, respectively, while the majority is sourced from the Southeastern pan handle. This study may be used to inform new science and guide future field studies that aim to assess local distributions and magnitudes, as well as their associated nutrient and solute flux. Such research is currently severely limited within the region. Fresh SGD is highly variable and difficult to measure but greatly important from a water resources and coastal ecology perspective. Our findings are especially relevant to identify where future studies that quantify the contribution of fresh SGD locally should take place.

Acknowledgments

We thank the anonymous reviewers for their thoughtful peer review. We would also like to thank C. Sergeant and J. Beamer for their assistance with accessing the Gulf of Alaska Hydrologic Model. Funding for this research was provided by the Alaska NSF EPSCoR (award #IA-1757348 to Lee Ann Munk and others). Furthermore, A. Russo would like to thank the UMass Department of Geosciences for funding his graduate research and providing scholarships for field visits to the Gulf of Alaska. The following data are available as individual files at Scholarworks@UA (http://hdl.handle.net/11122/13150):

- Source code for LPRM model (R file)
- Input and output files for LPRM and GLDAS models (.csv files)
- ESRI map package (.aprx file) that allows subsequent users to recreate Figures 3 and 5 using ArcGIS Pro
- A PythonAnywhere application to visualize fresh SGD timeseries for individual coastal catchments across the GoA domain (http://kbaystreamteam.pythonanywhere.com/apps/sgd)

Open Research

All data are available at Scholarworks@UA (http://hdl.handle.net/11122/13150).

826

827 **References**

828 Acker, J.G., and Leptoukh, G., 2007, Online analysis enhances use of NASA earth science data:
829 Eos, Transactions American Geophysical Union, v. 88, p. 14–17,
830 doi:10.1029/2007EO020003.
831 Adyasari, D., Hassenrück, C., Oehler, T., Sabdaningsih, A., and Moosdorf, N., 2019, Microbial
832 community structure associated with submarine groundwater discharge in northern Java
833 (Indonesia): Science of the Total Environment, v. 689, p. 590–601,
834 doi:10.1016/j.scitotenv.2019.06.193.
835 Andrisoa, A., Lartaud, F., Rodellas, V., Neveu, I., and Stieglitz, T.C., 2019, Enhanced growth
836 rates of the Mediterranean mussel in a coastal lagoon driven by groundwater inflow:
837 Frontiers in Marine Science, v. 6, p. 753, doi:10.3389/fmars.2019.00753.
838 Arendt, A., Echelmeyer, K.A., Harrison, W.D., Lingle, C.S., and Valentine, V.B., 2002, Rapid
839 wastage of Alaska glaciers and their contribution to rising sea level: Science, v. 297, p.
840 382–386, doi:10.1126/science.1072497.
841 Arp, C.D., Whitman, M.S., Kemnitz, R., and Stuefer, S.L., 2020, Evidence of hydrological
842 intensification and regime change from northern Alaskan watershed runoff: Geophysical
843 Research Letters, v. 47, p. e2020GL089186, doi:10.1029/2020GL089186.
844 Beamer, J.P., Hill, D.F., Arendt, A., and Liston, G.E., 2016, High-resolution modeling of coastal
845 freshwater discharge and glacier mass balance in the Gulf of Alaska watershed: Water
846 Resources Research, v. 52, p. 3888–3909, doi:10.1002/2015WR018457.
847 Beamer, J.P., Hill, D.F., Mcgrath, D., Arendt, A., and Kienholz, C., 2017, Hydrologic impacts of
848 changes in climate and glacier extent in the Gulf of Alaska watershed: Water Resources
849 Research, v. 53, p. 7502–7520, doi:10.1002/2016WR020033.
850 Beck, A.J., Charette, M.A., Cochran, J.K., Gonneea, M.E., and Peucker-Ehrenbrink, B., 2013,
851 Dissolved strontium in the subterranean estuary–implications for the marine strontium
852 isotope budget: Geochimica et Cosmochimica Acta, v. 117, p. 33–52,
853 doi:10.1016/j.gca.2013.03.021.
854 Beusen, A.H.W., Slomp, C.P., and Bouwman, A.F., 2013, Global land-ocean linkage: Direct
855 inputs of nitrogen to coastal waters via submarine groundwater discharge: Environmental
856 Research Letters, v. 8, doi:10.1088/1748-9326/8/3/034035.

857 Bieniek, P.A., Walsh, J.E., Thoman, R.L., and Bhatt, U.S., 2014, Using climate divisions to
858 analyze variations and trends in Alaska temperature and precipitation: Journal of Climate, v.
859 27, p. 2800–2818, doi:10.1175/JCLI-D-13-00342.1.
860 Boulton, G.S., and Caban, P., 1995, Groundwater flow beneath ice sheets: Part II — Its impact
861 on glacier tectonic structures and moraine formation: Quaternary Science Reviews, v. 14, p.
862 563–587, doi:10.1016/0277-3791(95)00058-W.
863 Bradley, D.C., and Kusky, T.M., 1990, Kinematics of late faults along Turnagain Arm, Mesozoic
864 accretionary complex, south-central Alaska: US Geological Survey Bulletin, v. 1946, p. 3–
865 10.
866 Brennan, S.R., Fernandez, D.P., Mackey, G., Cerling, T.E., Bataille, C.P., Bowen, G.J., and
867 Wooller, M.J., 2014, Strontium isotope variation and carbonate versus silicate weathering in
868 rivers from across Alaska: Implications for provenance studies: Chemical Geology, v. 389,
869 p. 167–181, doi:https://doi.org/10.1016/j.chemgeo.2014.08.018.
870 Brown, M.T., Lippiatt, S.M., and Bruland, K.W., 2010, Dissolved aluminum, particulate
871 aluminum, and silicic acid in northern Gulf of Alaska coastal waters: Glacial/riverine inputs
872 and extreme reactivity: Marine Chemistry, v. 122, p. 160–175,
873 doi:https://doi.org/10.1016/j.marchem.2010.04.002.
874 Bunn, A.G., Goetz, S.J., Kimball, J.S., and Zhang, K., 2007, Northern high-latitude ecosystems
875 respond to climate change: Eos, Transactions American Geophysical Union, v. 88, p. 333–
876 335, doi:10.1029/2007EO340001.
877 Burnett, W.C., Aggarwal, P.K., Aureli, A., Bokuniewicz, H., Cable, J.E., Charette, M.A., Kontar,
878 E., Krupa, S., Kulkarni, K.M., and Loveless, A., 2006, Quantifying submarine groundwater
879 discharge in the coastal zone via multiple methods: Science of the Total Environment, v.
880 367, p. 498–543, doi:10.1016/j.scitotenv.2006.05.009.
881 Charette, M.A., 2007, Hydrologic forcing of submarine groundwater discharge: Insight from a
882 seasonal study of radium isotopes in a groundwater-dominated salt marsh estuary:
883 Limnology and Oceanography, v. 52, p. 230–239, doi:10.4319/lo.2007.52.1.0230.
884 Chen, X., Lao, Y., Wang, J., Du, J., Liang, M., and Yang, B., 2018, Submarine groundwater-
885 borne nutrients in a tropical bay (Maowei Sea, China) and their impacts on the oyster
886 aquaculture: Geochemistry, Geophysics, Geosystems, v. 19, p. 932–951,
887 doi:10.1002/2017GC007330.

888 Chiang, J.C.H., and Bitz, C.M., 2005, Influence of high latitude ice cover on the marine
889 Intertropical Convergence Zone: Climate Dynamics, v. 25, p. 477–496,
890 doi:10.1007/s00382-005-0040-5.
891 Cyronak, T., Santos, I.R., Erler, D. V., and Eyre, B.D., 2013, Groundwater and porewater as
892 major sources of alkalinity to a fringing coral reef lagoon (Muri Lagoon, Cook Islands):
893 Biogeosciences, v. 10, p. 2467–2480, doi:10.5194/bg-10-2467-2013.
894 Dimova, N.T., Paytan, A., Kessler, J.D., Sparrow, K.J., Garcia-Tigreros Kodovska, F., Lecher,
895 A.L., Murray, J., and Tulaczyk, S.M., 2015, Current magnitude and mechanisms of
896 groundwater discharge in the Arctic: case study from Alaska: Environmental Science &
897 Technology, v. 49, p. 12036–12043, doi:10.1021/acs.est.5b02215.
898 Edwards, R.T., D'Amore, D. V., Biles, F.E., Fellman, J.B., Hood, E.W., Trubilowicz, J.W., and
899 Floyd, W.C., 2021, Riverine Dissolved Organic Carbon and Freshwater Export in the
900 Eastern Gulf of Alaska: Journal of Geophysical Research: Biogeosciences, v. 126, p.
901 e2020JG005725, doi:10.1029/2020JG005725.
902 Erler, D. V, Santos, I.R., Zhang, Y., Tait, D.R., Befus, K.M., Hidden, A., Li, L., and Eyre, B.D.,
903 2014, Nitrogen transformations within a tropical subterranean estuary: Marine Chemistry, v.
904 164, p. 38–47, doi:10.1016/j.marchem.2014.05.008.
905 Ferguson, G., and Gleeson, T., 2012, Vulnerability of coastal aquifers to groundwater use and
906 climate change: Nature climate change, v. 2, p. 342–345, doi:10.1038/NCLIMATE1413.
907 Fujita, K., Shoji, J., Sugimoto, R., Nakajima, T., Honda, H., Takeuchi, M., Tominaga, O., and
908 Taniguchi, M., 2019, Increase in fish production through bottom-up trophic linkage in
909 coastal waters induced by nutrients supplied via submarine groundwater: Frontiers in
910 Environmental Science, v. 7, p. 82, doi:10.3389/fenvs.2019.00082.
911 Gardner, A.S. et al., 2013, A Reconciled Estimate of Glacier Contributions to Sea Level Rise:
912 2003 to 2009: Science, v. 340, p. 852–857, doi:10.1126/science.1234532.
913 Van Genuchten, M.T., 1980, A closed-form equation for predicting the hydraulic conductivity of
914 unsaturated soils: Soil science society of America journal, v. 44, p. 892–898.
915 Gleeson, T., Moosdorf, N., Hartmann, J., and Van Beek, L.P.H., 2014, A glimpse beneath earth's
916 surface: GLobal HYdrogeology MaPS (GLHYMPS) of permeability and porosity:
917 Geophysical Research Letters, v. 41, p. 3891–3898, doi:doi.org/10.1002/2014GL059856.
918 Hagemann, S., 2002, An improved land surface parameter dataset for global and regional climate

models: Max-Planck-Institut für Meteorologie, doi:10.17617/2.2344576.

Hajati, M., Sutanudjaja, E., and Moosdorf, N., 2019, Quantifying Regional Fresh Submarine Groundwater Discharge With the Lumped Modeling Approach CoCa-RFSGD: Water Resources Research, v. 55, p. 5321–5341, doi:10.1029/2018WR024248.

He, Q., Kuang, X., Chen, J., Jiao, J.J., Liang, S., and Zheng, C., 2022, Subglacial meltwater recharge in the Dongkemadi River Basin, Yangtze River source region: Groundwater, v. 60, p. 434–450, doi:doi.org/10.1111/gwat.13189.

Heiss, J.W., and Michael, H.A., 2014, Tidal, spring-neap, and seasonal dynamics of a saltwater-freshwater mixing zone in a beach aquifer: Water Resources Research, v. 50, p. 6747–6766, doi:10.1002/2014WR015574.

Hill, D.F., Bruhis, N., Calos, S.E., Arendt, A., and Beamer, J., 2015, Spatial and temporal variability of freshwater discharge into the Gulf of Alaska: Journal of Geophysical Research: Oceans, v. 120, p. 634–646, doi:10.1002/2014JC010395.

Hood, E., Battin, T.J., Fellman, J., O'Neel, S., and Spencer, R.G.M., 2015, Storage and release of organic carbon from glaciers and ice sheets: Nature Geoscience, v. 8, p. 91–96, doi:10.1038/ngeo2331.

Hood, E., Fellman, J., Spencer, R.G.M., Hernes, P.J., Edwards, R., D'Amore, D., and Scott, D., 2009, Glaciers as a source of ancient and labile organic matter to the marine environment: Nature, v. 462, p. 1044–1047, doi:10.1038/nature08580.

Hu, C., Muller-Karger, F.E., and Swarzenski, P.W., 2006, Hurricanes, submarine groundwater discharge, and Florida's red tides: Geophysical Research Letters, v. 33, doi:10.1029/2005GL025449.

Jaeger, J.M., Nittrouer, C.A., Scott, N.D., and Milliman, J.D., 1998, Sediment accumulation along a glacially impacted mountainous coastline: north-east Gulf of Alaska: Basin Research, v. 10, p. 155–173, doi:10.1046/j.1365-2117.1998.00059.x.

Jenckes, J., Ibarra, D.E., and Munk, L.A., 2021, Concentration-Discharge Patterns Across the Gulf of Alaska Reveal Geomorphological and Glacierization Controls on Stream Water Solute Generation and Export: Geophysical Research Letters, v. 49, p. e2021GL095152, doi:10.1029/2021gl095152.

Klammler, H., Jawitz, J.W., Annable, M.D., Yaquian, J.A., Hatfield, K., and Burger, P., 2020, Decadal scale recharge-discharge time lags from aquifer freshwater-saltwater interactions:

Journal of Hydrology, v. 582, doi:10.1016/j.jhydrol.2019.124514.

Knee, K.L., and Paytan, A., 2012, Submarine Groundwater Discharge: A Source of Nutrients, Metals, and Pollutants to the Coastal Ocean, *in* Treatise on Estuarine and Coastal Science, Elsevier Inc., v. 4, p. 205–233, doi:10.1016/B978-0-12-374711-2.00410-1.

Kozeny, J., 1927, Über kapillare Leitung des Wassers im Boden-Aufstieg, Versickerung und Anwendung auf die Bewässerung, Sitzungsberichte der Akademie der Wissenschaften Wien: Mathematisch Naturwissenschaftliche Abteilung, v. 136, p. 271–306.

Kuan, W.K., Jin, G., Xin, P., Robinson, C., Gibbes, B., and Li, L., 2012, Tidal influence on seawater intrusion in unconfined coastal aquifers: Water Resources Research, v. 48, doi:10.1029/2011WR010678.

Larsen, C.F., Motyka, R.J., Freymueller, J.T., Echelmeyer, K.A., and Ivins, E.R., 2005, Rapid viscoelastic uplift in southeast Alaska caused by post-Little Ice Age glacial retreat: Earth and Planetary Science Letters, v. 237, p. 548–560, doi:10.1016/j.epsl.2005.06.032.

Lecher, A.L., Kessler, J., Sparrow, K., Garcia-Tigreros Kodovska, F., Dimova, N., Murray, J., Tulaczyk, S., and Paytan, A., 2016, Methane transport through submarine groundwater discharge to the North Pacific and Arctic Ocean at two Alaskan sites: Limnology and Oceanography, v. 61, p. S344–S355, doi:10.1002/lno.10118.

Lecher, A.L., and Mackey, K.R.M., 2018, Synthesizing the effects of submarine groundwater discharge on Marine Biota: Hydrology, v. 5, doi:10.3390/hydrology5040060.

Lecher, A.L., Mackey, K.R.M., and Paytan, A., 2017, River and Submarine Groundwater Discharge Effects on Diatom Phytoplankton Abundance in the Gulf of Alaska: Hydrology, v. 4, doi:10.3390/hydrology4040061.

Lehner, B., Verdin, K., and Jarvis, A., 2008, New global hydrography derived from spaceborne elevation data: Eos, Transactions American Geophysical Union, v. 89, p. 93–94, doi:10.1029/2008EO100001.

Van de Leur, D.A.K., 1958, A study of non-steady groundwater flow with special reference to a reservoir coefficient: De Ingenieur, v. 70, p. B87–B94.

Liljedahl, A.K., Gädeke, A., O'Neel, S., Gatesman, T.A., and Douglas, T.A., 2017, Glacierized headwater streams as aquifer recharge corridors, subarctic Alaska: Geophysical Research Letters, v. 44, p. 6876–6885, doi:10.1002/2017GL073834.

Liston, G.E., and Elder, K., 2006a, A distributed snow-evolution modeling system

(SnowModel): Journal of Hydrometeorology, v. 7, p. 1259–1276, doi:10.1175/JHM548.1.

Liston, G.E., and Elder, K., 2006b, A meteorological distribution system for high-resolution terrestrial modeling (MicroMet): Journal of Hydrometeorology, v. 7, p. 217–234, doi:10.1175/JHM486.1.

Liston, G.E., and Mernild, S.H., 2012, Greenland freshwater runoff. Part I: A runoff routing model for glaciated and nonglaciated landscapes (HydroFlow): Journal of Climate, v. 25, p. 5997–6014, doi:10.1175/JCLI-D-11-00591.1.

Loveland, T.R., Reed, B.C., Brown, J.F., Ohlen, D.O., Zhu, Z., Yang, L., and Merchant, J.W., 2000, Development of a global land cover characteristics database and IGBP DISCover from 1 km AVHRR data: International Journal of Remote Sensing, v. 21, p. 1303–1330, doi:10.1080/014311600210191.

Luijendijk, E., Gleeson, T., and Moosdorf, N., 2020, Fresh groundwater discharge insignificant for the world's oceans but important for coastal ecosystems: Nature Communications, v. 11, p. 1–12, doi:10.1038/s41467-020-15064-8.

Mackay, J.D., Barrand, N.E., Hannah, D.M., Krause, S., Jackson, C.R., Everest, J., MacDonald, A.M., and Ó Dochartaigh, B.É., 2020, Proglacial groundwater storage dynamics under climate change and glacier retreat: Hydrological Processes, v. 34, p. 5456–5473, doi:10.1002/hyp.13961.

Maizels, J.K., 1993, Quantitative regime modelling of fluvial depositional sequences: application to Holocene stratigraphy of humid-glacial braid-plains (Icelandic sandurs): Geological Society, London, Special Publications, v. 73, p. 53–78.

Mayfield, K.K., Eisenhauer, A., Ramos, D.P.S., Higgins, J.A., Horner, T.J., Auro, M., Magna, T., Moosdorf, N., Charette, M.A., and Gonneea, M.E., 2021, Groundwater discharge impacts marine isotope budgets of Li, Mg, Ca, Sr, and Ba: Nature Communications, v. 12, p. 1–9, doi:10.1038/s41467-020-20248-3.

McAfee, S.A., Guentchev, G., and Eischeid, J.K., 2013, Reconciling precipitation trends in Alaska: 1. Station-based analyses: Journal of Geophysical Research Atmospheres, v. 118, p. 7523–7541, doi:10.1002/jgrd.50572.

Michael, H.A., Charette, M.A., and Harvey, C.F., 2011, Patterns and variability of groundwater flow and radium activity at the coast: A case study from Waquoit Bay, Massachusetts: Marine Chemistry, v. 127, p. 100–114, doi:10.1016/j.marchem.2011.08.001.

1012 Michael, H.A., Mulligan, A.E., and Harvey, C.F., 2005, Seasonal oscillations in water exchange
1013 between aquifers and the coastal ocean: Nature, v. 436, p. 1145–1148,
1014 doi:10.1038/nature03935.
1015 Michael, H.A., Scott, K.C., Koneshloo, M., Yu, X., Khan, M.R., and Li, K., 2016, Geologic
1016 influence on groundwater salinity drives large seawater circulation through the continental
1017 shelf: Geophysical Research Letters, v. 43, p. 10,782-10,791, doi:10.1002/2016GL070863.
1018 Moore, W.S., 1999, The subterranean estuary: a reaction zone of ground water and sea water:
1019 Marine Chemistry, v. 65, p. 111–125, doi:10.1029/2019WR026554.
1020 Munro, J.M., and Gill, W.G., 2006, The Alaska Cruise Industry, *in* Cruise Ship Tourism, CABI,
1021 p. 145–159.
1022 Neal, E.G., Hood, E., and Smikrud, K., 2010, Contribution of glacier runoff to freshwater
1023 discharge into the Gulf of Alaska: Geophysical Research Letters, v. 37,
1024 doi:10.1029/2010GL042385.
1025 O'Neel, S., Hood, E., Bidlack, A.L., Fleming, S.W., Arimitsu, M.L., Arendt, A., Burgess, E.,
1026 Sergeant, C.J., Beaudreau, A.H., and Timm, K., 2015, Icefield-to-ocean linkages across the
1027 northern Pacific coastal temperate rainforest ecosystem: BioScience, v. 65, p. 499–512,
1028 doi:10.1093/biosci/biv027.
1029 Ó Dochartaigh, B.É., MacDonald, A.M., Black, A.R., Everest, J., Wilson, P., Darling, W.G.,
1030 Jones, L., and Raines, M., 2019, Groundwater–glacier meltwater interaction in proglacial
1031 aquifers: Hydrology and Earth System Sciences, v. 23, p. 4527–4539.
1032 Pelletier, J.D., Broxton, P.D., Hazenberg, P., Zeng, X., Troch, P.A., Niu, G., Williams, Z.C.,
1033 Brunke, M.A., and Gochis, D., 2016, Global 1-km gridded thickness of soil, regolith, and
1034 sedimentary deposit layers: ORNL DAAC, doi:10.3334/ORNLDAAC/1304.
1035 Peterson, R.N., Moore, W.S., Chappel, S.L., Viso, R.F., Libes, S.M., and Peterson, L.E., 2016, A
1036 new perspective on coastal hypoxia: The role of saline groundwater: Marine Chemistry, v.
1037 179, p. 1–11, doi:10.1016/j.marchem.2015.12.005.
1038 Pisternick, T., Lilkendey, J., Audit-Manna, A., Dumur Neelayya, D., Neehaul, Y., and Moosdorf,
1039 N., 2020, Submarine groundwater springs are characterized by distinct fish communities:
1040 Marine Ecology, v. 41, p. e12610, doi:10.1111/maec.12610.
1041 Portner, H.-O. et al., 2019, IPCC Special Report on the Ocean and Cryosphere in a Changing
1042 Climate:, doi:10.1017/9781009157964.

1043 Rahman, S., Tamborski, J.J., Charette, M.A., and Cochran, J.K., 2019, Dissolved silica in the
1044 subterranean estuary and the impact of submarine groundwater discharge on the global
1045 marine silica budget: Marine Chemistry, v. 208, p. 29–42,
1046 doi:10.1016/j.marchem.2018.11.006.
1047 Robinson, C.E., Xin, P., Santos, I.R., Charette, M.A., Li, L., and Barry, D.A., 2018,
1048 Groundwater dynamics in subterranean estuaries of coastal unconfined aquifers: Controls
1049 on submarine groundwater discharge and chemical inputs to the ocean: Advances in Water
1050 Resources, v. 115, p. 315–331, doi:10.1016/j.advwatres.2017.10.041.
1051 Rodell, M., Houser, P.R., Jambor, U.E.A., Gottschalck, J., Mitchell, K., Meng, C.-J., Arsenault,
1052 K., Cosgrove, B., Radakovich, J., and Bosilovich, M., 2004, The global land data
1053 assimilation system: Bulletin of the American Meteorological society, v. 85, p. 381–394.
1054 Rodellas, V., Garcia-Orellana, J., Masqué, P., Feldman, M., Weinstein, Y., and Boyle, E.A.,
1055 2015, Submarine groundwater discharge as a major source of nutrients to the Mediterranean
1056 Sea: Proceedings of the National Academy of Sciences of the United States of America, v.
1057 112, p. 3926–3930, doi:10.1073/pnas.1419049112.
1058 Ronayne, M.J., Houghton, T.B., and Stednick, J.D., 2012, Field characterization of hydraulic
1059 conductivity in a heterogeneous alpine glacial till: Journal of Hydrology, v. 458–459, p.
1060 103–109, doi:10.1016/j.jhydrol.2012.06.036.
1061 Royer, T.C., 1982, Coastal fresh water discharge in the northeast Pacific: Journal of Geophysical
1062 Research: Oceans, v. 87, p. 2017–2021.
1063 Santos, I.R., Chen, X., Lecher, A.L., Sawyer, A.H., Moosdorf, N., Rodellas, V., Tamborski, J.,
1064 Cho, H.-M., Dimova, N., and Sugimoto, R., 2021, Submarine groundwater discharge
1065 impacts on coastal nutrient biogeochemistry: Nature Reviews Earth & Environment, v. 2, p.
1066 307–323, doi:10.1038/s43017-021-00152-0.
1067 Santos, I.R., Dimova, N., Peterson, R.N., Mwashote, B., Chanton, J., and Burnett, W.C., 2009,
1068 Extended time series measurements of submarine groundwater discharge tracers (222Rn
1069 and CH4) at a coastal site in Florida: Marine Chemistry, v. 113, p. 137–147,
1070 doi:10.1016/j.marchem.2009.01.009.
1071 Sawyer, A.H., David, C.H., and Famiglietti, J.S., 2016, Continental patterns of submarine
1072 groundwater discharge reveal coastal vulnerabilities Downloaded from: Science, v. 353, p.
1073 705–707, doi:10.5281/zenodo.58871.

1074 Schroth, A.W., Crusius, J., Chever, F., Bostick, B.C., and Rouxel, O.J., 2011, Glacial influence
1075 on the geochemistry of riverine iron fluxes to the Gulf of Alaska and effects of deglaciation:
1076 Geophysical Research Letters, v. 38, doi:10.1029/2011GL048367.
1077 Sergeant, C.J., Falke, J.A., Bellmore, R.A., Bellmore, J.R., and Crumley, R.L., 2020, A
1078 Classification of Streamflow Patterns Across the Coastal Gulf of Alaska: Water Resources
1079 Research, v. 56, doi:10.1029/2019WR026127.
1080 Sheffield, J., Goteti, G., and Wood, E.F., 2006, Development of a 50-year high-resolution global
1081 dataset of meteorological forcings for land surface modeling: Journal of climate, v. 19, p.
1082 3088–3111.
1083 Simons, G., Koster, R., and Droogers, P., 2020, Hihydrosoil v2. 0-high resolution soil maps of
1084 global hydraulic properties: FutureWater Report 213.
1085 Slomp, C.P., and Van Cappellen, P., 2004, Nutrient inputs to the coastal ocean through
1086 submarine groundwater discharge: controls and potential impact: Journal of Hydrology, v.
1087 295, p. 64–86, doi:10.1016/j.jhydrol.2004.02.018.
1088 Smith, C.G., Cable, J.E., Martin, J.B., and Roy, M., 2008, Evaluating the source and seasonality
1089 of submarine groundwater discharge using a radon-222 pore water transport model: Earth
1090 and Planetary Science Letters, v. 273, p. 312–322, doi:10.1016/j.epsl.2008.06.043.
1091 Somers, L.D., and McKenzie, J.M., 2020, A review of groundwater in high mountain
1092 environments: Wiley Interdisciplinary Reviews: Water, v. 7, p. e1475,
1093 doi:10.1002/wat2.1475.
1094 Somers, L.D., McKenzie, J.M., Mark, B.G., Lagos, P., Ng, G.H.C., Wickert, A.D., Yarleque, C.,
1095 Baraër, M., and Silva, Y., 2019, Groundwater Buffers Decreasing Glacier Melt in an
1096 Andean Watershed—But Not Forever: Geophysical Research Letters, v. 46, p. 13016–
1097 13026, doi:10.1029/2019GL084730.
1098 Spalt, N., Murgulet, D., and Abdulla, H., 2020, Spatial variation and availability of nutrients at
1099 an oyster reef in relation to submarine groundwater discharge: Science of The Total
1100 Environment, v. 710, p. 136283, doi:10.1016/j.scitotenv.2019.136283.
1101 Starke, C., Ekau, W., and Moosdorf, N., 2020, Enhanced productivity and fish abundance at a
1102 submarine spring in a coastal lagoon on Tahiti, French Polynesia: Frontiers in Marine
1103 Science, v. 6, p. 809, doi:10.3389/fmars.2019.00809.
1104 Stopha, M.E., 2017, Alaska fisheries enhancement annual report 2016: Alaska Department of

Fish and Game, Division of Commercial Fisheries Anchorage.

Sugimoto, R., Honda, H., Kobayashi, S., Takao, Y., Tahara, D., Tominaga, O., and Taniguchi, M., 2016, Seasonal Changes in Submarine Groundwater Discharge and Associated Nutrient Transport into a Tideless Semi-enclosed Embayment (Obama Bay, Japan): Estuaries and Coasts, v. 39, p. 13–26, doi:10.1007/s12237-015-9986-7.

Swarzenski, P.W., Reich, C., Kroeger, K.D., and Baskaran, M., 2007a, Ra and Rn isotopes as natural tracers of submarine groundwater discharge in Tampa Bay, Florida: Marine Chemistry, v. 104, p. 69–84, doi:10.1016/j.marchem.2006.08.001.

Swarzenski, P.W., Simonds, F.W., Paulson, A.J., Kruse, S., and Reich, C., 2007b, Geochemical and geophysical examination of submarine groundwater discharge and associated nutrient loading estimates into lynch cove, Hood Canal, WA: Environmental Science and Technology, v. 41, p. 7022–7029, doi:10.1021/es070881a.

Syed, T.H., Famiglietti, J.S., and Chambers, D.P., 2009, GRACE-based estimates of terrestrial freshwater discharge from basin to continental scales: Journal of Hydrometeorology, v. 10, p. 22–40, doi:10.1175/2008JHM993.1.

Tamborski, J.J., Rogers, A.D., Bokuniewicz, H.J., Cochran, J.K., and Young, C.R., 2015, Identification and quantification of diffuse fresh submarine groundwater discharge via airborne thermal infrared remote sensing: Remote Sensing of Environment, v. 171, p. 202–217, doi:10.1016/j.rse.2015.10.010.

Taniguchi, M., 2002, Tidal effects on submarine groundwater discharge into the ocean: Geophysical Research Letters, v. 29, p. 1–2, doi:10.1029/2002GL014987.

Taniguchi, M., Burnett, W.C., Cable, J.E., and Turner, J. V., 2002, Investigation of submarine groundwater discharge: Hydrological Processes, v. 16, p. 2115–2129, doi:10.1002/hyp.1145.

Taniguchi, M., Dulai, H., Burnett, K.M., Santos, I.R., Sugimoto, R., Stieglitz, T., Kim, G., Moosdorf, N., and Burnett, W.C., 2019, Submarine groundwater discharge: updates on its measurement techniques, geophysical drivers, magnitudes, and effects: Frontiers in Environmental Science, v. 7, p. 141, doi:10.3389/fenvs.2019.00141.

Wang, J., Jin, M., Musgrave, D.L., and Ikeda, M., 2004, A hydrological digital elevation model for freshwater discharge into the Gulf of Alaska: Journal of Geophysical Research: Oceans, v. 109, p. 1–15, doi:10.1029/2002JC001430.

1136 Weingartner, T.J., Danielson, S.L., and Royer, T.C., 2005, Freshwater variability and
1137 predictability in the Alaska Coastal Current: Deep Sea Research Part II: Topical Studies in
1138 Oceanography, v. 52, p. 169–191, doi:10.1016/j.dsr2.2004.09.030.
1139 Wilson, F.H., and Labay, K.A., 2016, Alaska geology revealed: US Geological Survey.
1140 Wilson, J., and Rocha, C., 2012, Regional scale assessment of Submarine Groundwater
1141 Discharge in Ireland combining medium resolution satellite imagery and geochemical
1142 tracing techniques: Remote Sensing of Environment, v. 119, p. 21–34,
1143 doi:10.1016/j.rse.2011.11.018.
1144 Xin, P., Robinson, C., Li, L., Barry, D.A., and Bakhtyar, R., 2010, Effects of wave forcing on a
1145 subterranean estuary: Water Resources Research, v. 46, doi:10.1029/2010WR009632.
1146 Yu, X., Xu, Z., Moraetis, D., Nikolaidis, N.P., Schwartz, F.W., Zhang, Y., Shu, L., Duffy, C.J.,
1147 and Liu, B., 2021, Capturing hotspots of fresh submarine groundwater discharge using a
1148 coupled surface–subsurface model: Journal of Hydrology, v. 598, p. 126356,
1149 doi:https://doi.org/10.1016/j.jhydrol.2021.126356.
1150 Zhou, Y., Befus, K.M., Sawyer, A.H., and David, C.H., 2018, Opportunities and challenges in
1151 computing fresh groundwater discharge to continental coastlines: a multimodel comparison
1152 for the United States Gulf and Atlantic Coasts: Water Resources Research, v. 54, p. 8363–
1153 8380, doi:10.1029/2018WR023126.
1154 Zhou, Y., Sawyer, A.H., David, C.H., and Famiglietti, J.S., 2019, Fresh submarine groundwater
1155 discharge to the near-global coast: Geophysical Research Letters, v. 46, p. 5855–5863,
1156 doi:10.1029/2019GL082749.
1157